

## Article

# Valorization of Different Fractions from Butiá Pomace by Pyrolysis: H<sub>2</sub> Generation and Use of the Biochars for CO<sub>2</sub> Capture

 Isaac dos S. Nunes <sup>1</sup>, Carlos Schnorr <sup>2</sup>, Daniele Perondi <sup>3</sup>, Marcelo Godinho <sup>3</sup>, Julia C. Diel <sup>1</sup>, Lauren M. M. Machado <sup>1</sup>, Fabíola B. Dalla Nora <sup>1</sup>, Luis F. O. Silva <sup>2,\*</sup> and Guilherme L. Dotto <sup>1,\*</sup>

- <sup>1</sup> Research Group on Adsorptive and Catalytic Process Engineering (ENGEPAC), Federal University of Santa Maria, Roraima Avenue, 1000-7, Santa Maria 97105-900, Brazil
- <sup>2</sup> Department of Natural and Exact Sciences, Universidad de la Costa, CUC, Calle 58 # 55-66, Barranquilla 080002, Colombia
- <sup>3</sup> Postgraduate Program in Engineering Processes and Technology, University of Caxias do Sul—UCS, Caxias do Sul 95070-560, Brazil
- \* Correspondence: lsilva8@cuc.edu.co (L.F.O.S.); guilherme\_dotto@yahoo.com.br (G.L.D.)

**Abstract:** This work valorizes butiá pomace (*Butia capitata*) using pyrolysis to prepare CO<sub>2</sub> adsorbents. Different fractions of the pomace, like fibers, endocarps, almonds, and deoiled almonds, were characterized and later pyrolyzed at 700 °C. Gas, bio-oil, and biochar fractions were collected and characterized. The results revealed that biochar, bio-oil, and gas yields depended on the type of pomace fraction (fibers, endocarps, almonds, and deoiled almonds). The higher biochar yield was obtained by endocarps (31.9%wt.). Furthermore, the gas fraction generated at 700 °C presented an H<sub>2</sub> content higher than 80%vol regardless of the butiá fraction used as raw material. The biochars presented specific surface areas reaching 220.4 m<sup>2</sup> g<sup>-1</sup>. Additionally, the endocarp-derived biochar presented a CO<sub>2</sub> adsorption capacity of 66.43 mg g<sup>-1</sup> at 25 °C and 1 bar, showing that this material could be an effective adsorbent to capture this greenhouse gas. Moreover, this capacity was maintained for 5 cycles. Biochars produced from butiá precursors without activation resulted in a higher surface area and better performance than some activated carbons reported in the literature. The results highlighted that pyrolysis could provide a green solution for butiá agro-industrial wastes, generating H<sub>2</sub> and an adsorbent for CO<sub>2</sub>.

**Keywords:** butiá wastes; pyrolysis; butiá biochar; H<sub>2</sub> generation; CO<sub>2</sub> adsorption



**Citation:** Nunes, I.d.S.; Schnorr, C.; Perondi, D.; Godinho, M.; Diel, J.C.; Machado, L.M.M.; Dalla Nora, F.B.; Silva, L.F.O.; Dotto, G.L. Valorization of Different Fractions from Butiá Pomace by Pyrolysis: H<sub>2</sub> Generation and Use of the Biochars for CO<sub>2</sub> Capture. *Molecules* **2022**, *27*, 7515. <https://doi.org/10.3390/molecules27217515>

Academic Editors: Ines Matos, Maria Bernardo and Elena Perez Mayoral

Received: 27 September 2022

Accepted: 29 October 2022

Published: 3 November 2022

**Publisher's Note:** MDPI stays neutral with regard to jurisdictional claims in published maps and institutional affiliations.



**Copyright:** © 2022 by the authors. Licensee MDPI, Basel, Switzerland. This article is an open access article distributed under the terms and conditions of the Creative Commons Attribution (CC BY) license (<https://creativecommons.org/licenses/by/4.0/>).

## 1. Introduction

Pollution is one of the major global issues regarding the environment. The main source of this problem is greenhouse gas emissions [1]. Industrialization and the combustion of coal and fossil fuels result in the emission of greenhouse and toxic gases [2], such as carbon dioxide (CO<sub>2</sub>), which causes harm to human health, and also contributes to global warming [3]. The increased CO<sub>2</sub> concentrations in the atmosphere have warmed the planet substantially [4]. Recent measurements found a mean concentration of 400 ppm [5–7] representing an elevation of 100 ppm compared to its pre-industrial time [8]. Therefore, reducing greenhouse gas emissions is one of the greatest global challenges through 2050 [9].

There are different methods to remove carbon dioxide, including absorption [10], cryogenic separation [11], membrane [12], and adsorption [13–17]. Adsorption is a favorable method due to its simple operation, low energy consumption, and low equipment cost [18]. This technology has been regarded as one of the most promising for mitigating greenhouse gases [19]. Adsorbents for CO<sub>2</sub> show advantages such as wider temperature range operation, less harmful disposal, yield, less waste generation, and weak bonding with CO<sub>2</sub>, resulting in lower regeneration energy [20]. Among different materials for CO<sub>2</sub> adsorption, such as activated carbon (AC) [13,21–23], biomass/biowaste [24,25], zeolite [26,27],

graphene [28], metal-organic frameworks [29,30], biochar [31,32] has been highlighted in recent years.

Biochar is the solid fraction obtained from biomass pyrolysis [33]. Besides biochar, pyrolysis generates non-condensable gases (CO, CO<sub>2</sub>, CH<sub>4</sub>, and H<sub>2</sub>) and condensable gases (bio-oil/liquid phase) [34]. Biochar presents a porous structure with abundant functional groups on the surface [35,36]. Producing biochar using waste biomass as a precursor is an effective process for converting waste into a high-value-added product [37]. The use of biomass has emerged as a promising low-cost solution [38] for the treatment and management of large volumes of agro-industrial wastes [39,40]. In this sense, biochar comes from a wide range of biomass, such as fruit, legume peels and husks [41–45], bagasse/pomace, fruit pit and shells [46–50], forestry wastes and pruning [51–53], sludge [54,55] and animal manure [56,57]. The biochar obtention releases more hydrogen than it consumes, making it a negative-emission technology [58]. This technology could be one cost-effective and environmentally friendly method for mitigating climate change [19] and pollution from inappropriate solid waste management.

The genus *Butia* belongs to the *Arecaceae* family, is native to South America, occur naturally in Brazil, Uruguay, Argentina, and Paraguay, and has great potential for expansion. Brazil retains the majority of species, and the occurrence spans Bahia, Santa Catarina, and Goiás, but most populations are found in the Rio Grande do Sul [59]. Butiá fruits as food are ancestral and are consumed fresh or used as culinary ingredients in juice, jelly, ice cream, yogurts, sweets, flour, and liquor [60–63]. Processing native fruits, such as butiá, is an economic activity for smallholders and farmers [60] that offers the highest potential for income generation [64]. The pulp contains high concentrations of vitamins (C and A), fibers, and phenolic compounds, potentially expanding the agro-industrial use of the fruits [61]. In addition, extracts of butiá fruits have shown potential antimicrobial properties [65,66]. Seed oil was studied to produce biofuel [67,68] and antibiofilm activity [69]. Besides the fruits and leaves used, the seeds are usually discarded [70], motivating studies to recover this waste.

Sustainable use of butiá palm groves could increase family incomes and result in social and environmental dividends [60]. However, this development would generate agro-industrial solid wastes that need appropriate treatment for energy generation or producing material for environmental regeneration. Recent studies have reported butiá endocarps [71,72]. However, no works were founded employing other fractions from butiá wastes, such as fibers and almonds, as a precursor of adsorbents, highlighting this work's scientific contribution/novelty. Considering air and soil pollution, from the perspective of sustainable development, it is interesting to obtain solid biochar from butiá wastes that can capture CO<sub>2</sub>.

In this paper, butiá agro-industrial wastes were pyrolyzed, aiming to produce biochar for CO<sub>2</sub> adsorption. The pomace obtained in familiar agroindustry was separated into four precursors (fibers, endocarps, almonds, and deoiled almonds). The pyrolysis was conducted at 700 °C, and the yield of solid, liquid, and gaseous fractions was evaluated. Furthermore, the precursors and the pyrolysis products were characterized. Finally, the potential of the produced biochar for CO<sub>2</sub> adsorption was studied.

## 2. Results and Discussion

### 2.1. Features of the Butiá Precursors

Table 1 shows the characterization of four precursors separated from butiá pomace. The moisture content for precursors ranged from 5.19 to 6.06%wt. It was similar to other lignocellulosic biomasses such as switchgrass (6.25%wt.) [73] and palm fiber (4.23%wt.) previously dried in the thermochemical process [74]. Moreover, the results for butiá precursors were lower than tucumã seed (7.6%wt.) [75], almond and walnut shell (7.7 and 11%wt.) [76], and açai seeds [77], which are similar biomasses. The difference observed could be explained by the dry process initially used for butiá biomass conservation. Moisture content less than 10%wt. is desirable for biomass conversion in thermochemical processes [78].

**Table 1.** Proximate analysis results and cellulose, hemicellulose, and lignin composition for the butiá precursors.

Proximate Analysis *				
	FIB	END	ALM	DOA
Moisture (%wt.)	5.48 ± 0.08	5.19 ± 0.20	5.22 ± 1.44	6.06 ± 0.19
Ash (%wt.)	1.72 ± 0.08	0.51 ± 0.02	1.15 ± 0.06	2.25 ± 0.14
Fixed carbon (%wt.)	22.25 ± 0.58	25.6 ± 0.41	7.62 ± 0.42	12.13 ± 0.06
Volatile matter (%wt.)	76.03 ± 0.51	74.06 ± 0.27	91.23 ± 0.41	85.62 ± 0.18
Chemical Composition *				
	FIB	END	ALM	DOA
Cellulose (%wt.)	5.94 ± 0.68	6.14 ± 1.35	10.57 ± 0.38	57.79 ± 0.39
Hemicellulose (%wt.)	29.00 ± 1.14	24.34 ± 1.17	8.03 ± 0.36	11.81 ± 0.44
Lignin (%wt.)	15.32 ± 0.34	48.14 ± 1.44	19.12 ± 1.14	10.80 ± 0.85
Extractive (%wt.)	11.10 ± 0.65	7.44 ± 0.38	36.62 ± 1.14	1.35 ± 0.35

\* All results are mean ± standard error for  $n = 3$ .

Ash content presented in the literature on another lignocellulosic material range from 0.25 to 2.82%wt. [59,74,76,79]. In this work, the samples FIB and ALM presented similar ash content to tucumã (1.45%wt.) [75], açai seeds (1.36%wt.) [80] and almond shells (1.30%wt.) [81]. Comparing DOA with ALM, the higher content of ashes could be explained by the oil extraction from almonds, resulting in a higher presence of ashes (2.25%wt.) and a lower percentage of extractives (1.35%wt.).

For good power generation potential, the fixed carbon content should range from 15 to 25%wt. for efficient burning [82]. As can be seen in Table 1, samples FIB and END presented fixed carbon at this range and showed agreement with rubber seed shells (23.4%wt.) [83], avocado stone (22.4%wt.) [84] and Brazilian nut (25.21%wt.) [85]. Otherwise, samples ALM and DOA following rice straw (8.1%wt.) [86], sawdust (7.74%wt.) [87], and algae (12.8%wt.) [88]. Low ash content and high fixed carbon show that biomass is a potential candidate for bioenergy production [89]. Among the evaluated materials, FIB and END showed the greatest potential for this.

Related to volatile matter (Table 1), Aguiar et al. (2014) [90] reported that in butiá fruits, this parameter depends on maturation grade, climatic conditions, storage time and conditions, and specie of plant. The volatile matter results (Table 1) for the samples FIB and END corroborated tucumã (78.64%wt.) [75], banana trunk (74.33%wt.) [91], and olive kernel (75.8%wt.) [32], while DOA is near to the content of palm shells (62–85%wt.) [92], which has high oil yield like butiá almonds and palm fibers (86.51%wt.) [93] and ALM is near sawdust (90.92%wt.).

Table 1 revealed that the DOA sample resulted from a higher cellulose content. END presented higher lignin, while FIB had the major hemicellulose content. Percentages of hemicellulose and lignin obtained for FIB are comparable to wheat straw (23 to 30%wt. and 12 to 16%wt.), rice husk (12 to 29.3%wt. and 15.4 to 20%wt.), and sugarcane bagasse (12 to 29.3% and 1.4 to 20%wt.) [94]. END presented similar hemicellulose and lignin content to palm kernel shells (23.82 and 45.59%wt., respectively) [95]. ALM sample showed lignin content comparable to tucumã seeds (19.91%wt.) [77], hemicellulose content, and extractive similar to the almond hull (9.0 and 36.25%wt., respectively) [96].

Thermogravimetric curves (TG) and derivatives from the thermogravimetric curve (DTG) are shown in Figure 1a–d. The TG/DTG curves presented a consistent profile for lignocellulosic biomass. At different stages of weight loss, peaks in DTG curves can be seen that refer to the release of water or volatile organic compounds and thermo-decomposition of cellulose, hemicellulose, and lignin [77]. Weight losses observed until 184 °C can be attributed to water evaporation and degradation of organic compounds biomasses, as Baroni et al. (2015) [75]. For temperatures above 200 °C, the behavior of DTG curves is

predominantly exothermic due to the decomposition of hemicellulose, cellulose, and lignin into four precursors.

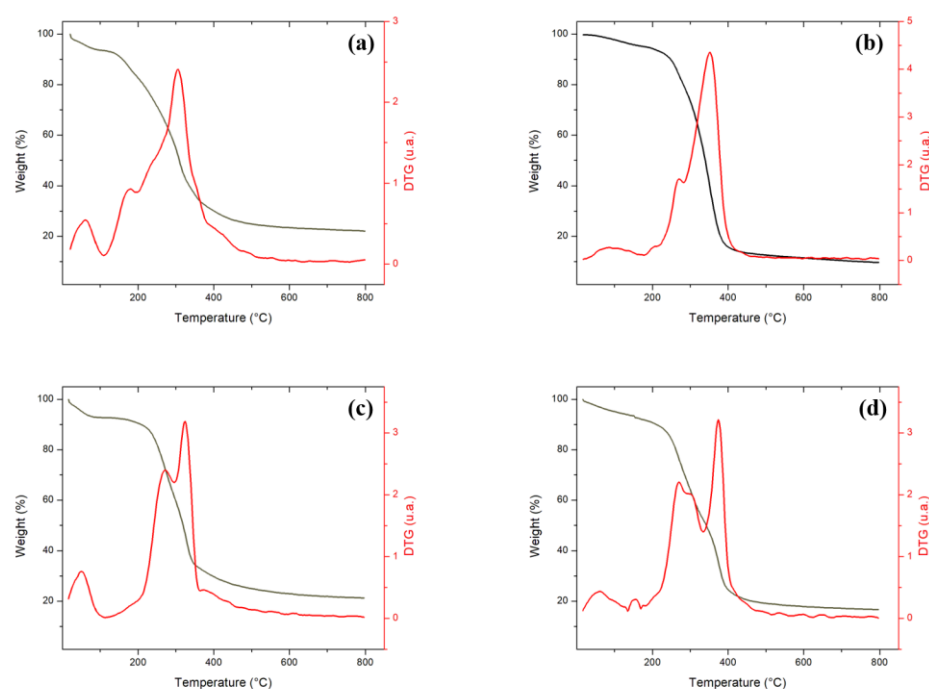


**Figure 1.** Thermogravimetric and derived curves to precursors (a) FIB, (b) ALM, (c) END, and (d) DOA.

Comparing the samples, FIB (Figure 1a), which has the higher hemicellulose content (Table 1), starts the thermal degradation at a lower temperature. Yang et al. (2007) [97] reported that this component starts its degradation in the range of 220 to 315 °C. Poletto et al. (2012) [98] detected hemicellulose degradation by a DTG peak near 300 °C. In this work, this peak is observed in DTG curves for the four precursors but is most pronounced in FIB (Figure 1a) and DOA (Figure 1d). END (Figure 1c) has a higher lignin content, which may explain the lower weight loss, remaining 21.3%wt. of the sample at the final temperature (800 °C). The remaining mass is similar to the açai seed (21.6%wt.), as Santos et al. (2020) [77] observed. Lignin is the major component of converting lignocellulosic wastes to char by its thermal resistance [97]. This component is responsible for delaying degradation [34], although this process starts at lower temperatures, in a wide range, from 160 to 900 °C [97]. END has pronounced hemicellulose content (Table 1) and presented (Figure 1c) degradation at 207 °C, with two peaks, at 270 and 322 °C. Perondi et al. (2017) [34] detected hemicellulose degradation from 260 to 400 °C, which is near the limit (410 °C) reported by Santos et al. (2020) [77].

ALM is the precursor with the highest cellulose content (Table 1) and starts degradation at 220 °C (Figure 1b), presenting peaks at 265 and 377 °C. The interval from 310 to 405 °C corresponds to 53.6% of losing weight. Subsequently, from 405 °C in a large range until 800 °C, the weight loss rate reduces drastically, which could be associated with lignin degradation (Perondi et al. 2017) [34].

The FTIR vibrational spectra of butiá precursors are reported in Figure S1a–d (Supplementary Material). All the precursors showed bands at 3400  $\text{cm}^{-1}$  that can be attributed to the O–H stretching vibrations of carboxylic acids, alcohols, phenols, or adsorbed water [99–101]. The four precursors exhibited bands at 2925 and 2854  $\text{cm}^{-1}$  that can be assigned to C–H stretch [72,97,102]. At 1745  $\text{cm}^{-1}$ , samples ALM (Figure S1b) and END (Figure S1c) presented a more pronounced band, attributed to O–H stretch and C=O stretching vibration from carbonyl/carboxylic acid [102]. These samples have the highest lignin content (Table 1) and presented a more intense band at 1457  $\text{cm}^{-1}$ . This signal is

attributed to the CH<sub>2</sub> stretching deformation of lignin [103]. All the precursors present a band at 1160 cm<sup>-1</sup>, assigned to asymmetric stretching C–O–C in cellulose [103]. The band at 1040 cm<sup>-1</sup> is related to the C–O stretch in carbohydrates (cellulose, hemicellulose, and lignin) [91,104]. Vibrations between 450 and 900 cm<sup>-1</sup> are characteristic of aromatic ring C–C stretching [91].

XRD diffraction patterns are shown in the supplementary material (Figure S2), and no crystalline phase was observed in all precursors. Then, it can be stated that butiá endocarps, fiber, almonds, and deoiled almonds have an amorphous structure. The supplementary material also presents SEM micrographs of FIB, END, and DOA (Figure S3). The micrographs presented roughness at the surface for FIB and cavities for END and DOA samples. The high oil content in ALM made SEM analysis impossible for this sample.

## 2.2. Results of the Pyrolysis Process

The product yields obtained from the butiá precursor's pyrolysis (END, FIB, ALM, and DOA) are shown in Figure 2. The sample END presented the highest biochar yield (31.9%wt.) due to its major lignin content. Lignin fragments have multiple aromatic rings that crosspolymerize to form more carbonaceous solids [105]. According to Wan et al. (2022) [40], lignin presents lower degradation as a consequence of its thermal resistance, resulting in a higher amount of biochar [20]. Sample ALM resulted in a higher bio-oil yield (72.2%wt.). This result may be explained by the high content of oil available in butiá almonds, ranging from 30 to 57.8%wt. [69,106,107] Considering their composition (Table 1), DOA and ALM presented the highest volatile matter content. Ahmad et al. (2017) [78] reported that a high content of volatile matter is expected to favor the formation of liquid and gaseous in pyrolysis. The ALM sample showed the highest bio-oil yield and, consequently, the lowest biochar yield (12.1%wt.). Low solid yield can make it unfeasible when the pyrolysis intends to obtain adsorbents. In addition, the oil obtained from butiá almonds extracted by hexane has anti-biofouling properties against total microorganisms, aciduric bacteria, lactobacilli, and *Streptococcus mutans* [108]. Butiá almond oil extracted by hexane has also been studied to produce biofuels [67,68]. DOA pyrolysis yielded a better biochar yield (19.8%wt.) than ALM.

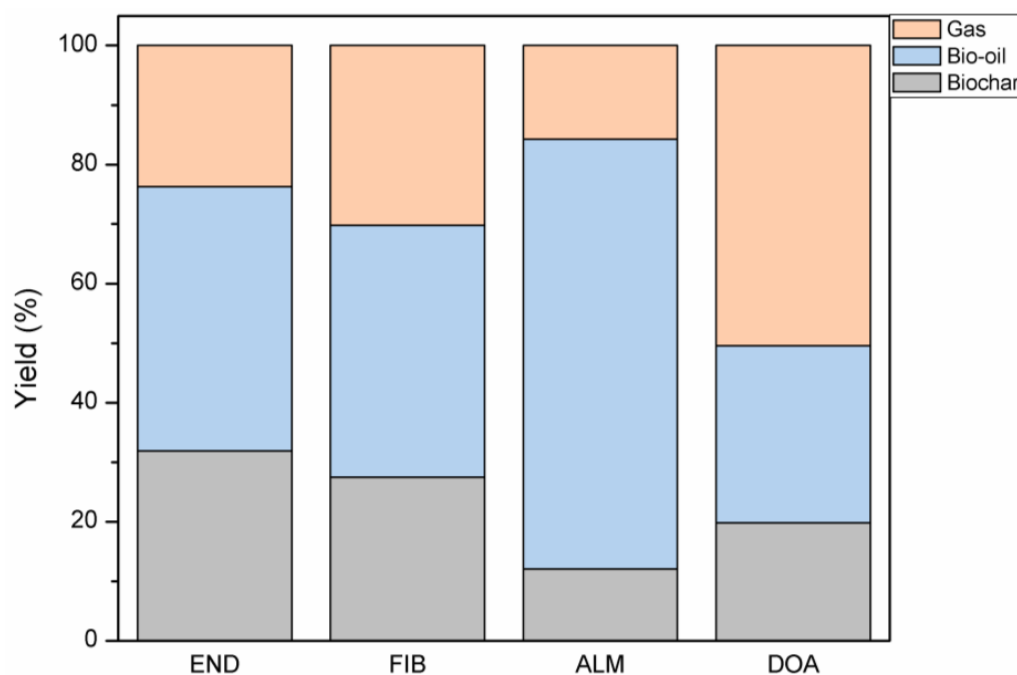
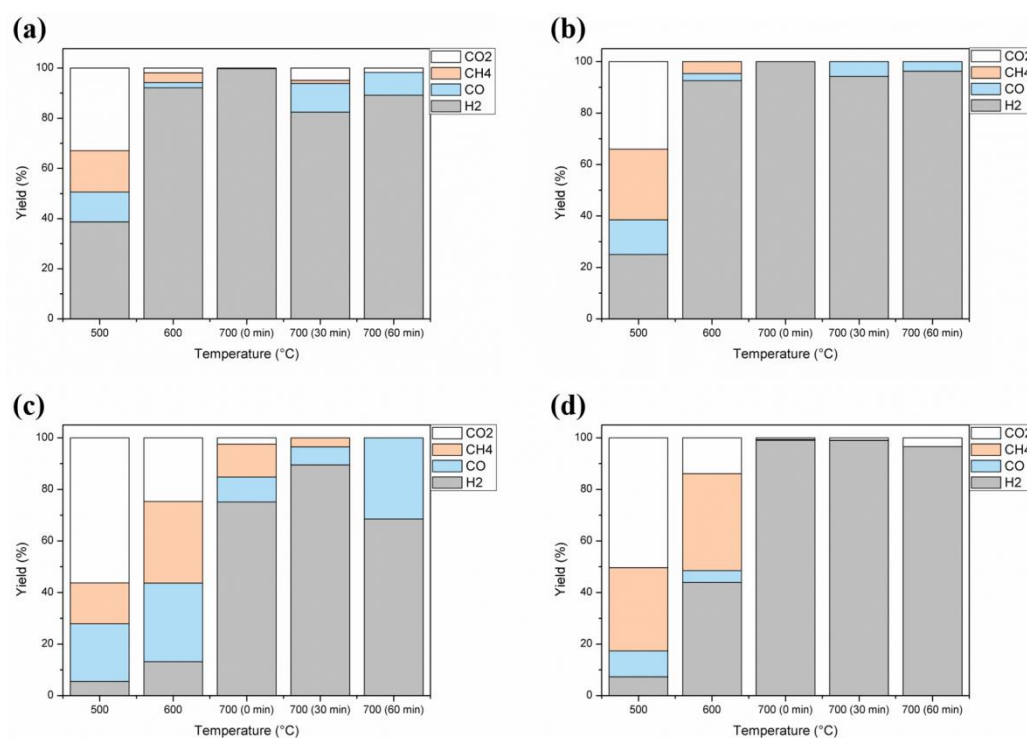


Figure 2. Product yields from pyrolysis of END, FIB, ALM, and DOA at 700 °C.

The increase in the cellulose and hemicellulose content leads to higher production of volatile vapor in pyrolysis [20]. This observation explains why DOA (69.6%wt. of cellulose and hemicellulose) had the highest gas production, reaching 50.5%wt. In addition, in pyrolysis, cellulose produces more fragments of smaller molecular sizes, increasing liquid and gaseous fractions [105].

### 2.3. Non-Condensable Gases Generation

Regarding gas production, Figure 3 presents the distribution of non-condensable gases affected by temperature. For all precursors, the major gas produced is H<sub>2</sub> which tends to increase in generation with temperature. This tendency was also observed by Perondi et al. (2017) and De Conto et al. (2016) [34,109]. Nevertheless, compared to other samples employed in this work, only END (Figure 3c) still increased H<sub>2</sub> generation 30 min after reaching the isotherm temperature (700 °C). This trend is attributed to lignin decomposition [97]. The H<sub>2</sub> generation should be highlighted since it is a green gas and could be used as a fuel.



**Figure 3.** Effect of temperature on gas production during the pyrolysis of (a) FIB, (b) ALM, (c) END, and (d) DOA.

CO generation was favored at lower temperatures until 600 °C, highlighted by sample END, and can be assigned to the thermal decomposition of hemicellulose [97]. At 700 °C, CO generation is observed for FIB (Figure 3a), ALM (Figure 3b) and END (Figure 3c). This observation can be related to the second pyrolysis of solid material and lignin degradation [97].

CH<sub>4</sub> generation was observed mainly until 600 °C, by degradation of the methoxyl group, decreasing after 700 °C. END sample (Figure 3c) released CH<sub>4</sub> at 700 °C (at 0 and 30 min) to the high content of lignin [34]. This tendency was also confirmed by De Conto et al. (2016) [109].

For CO<sub>2</sub> production, it was observed that it decreases with temperature, following Chang et al. (2016) [110]. Yang et al. (2007) [97] demonstrate that 500 °C results in higher CO<sub>2</sub> production. However, CO<sub>2</sub> releases still at 600 °C and 700 °C (Figure 3c), which can be attributed to hemicellulose, but majorly, lignin degradation [97].

#### 2.4. Biochars Characteristics

Figure S4 (Supplementary Material) shows FTIR results obtained from biochars. For all biochars, the bands' intensity indicated a strong reduction. Similar behavior was observed previously [99,100]. For example, in Figure S4, it can be seen that a band assigned to O–H stretching vibration remained [97]. Additionally, some bands around 1700  $\text{cm}^{-1}$  remained. In general, the amount and intensity of the bands decreased after pyrolysis operation regardless of precursors. This trend results from volatilizing a great fraction of the precursors during the thermochemical process. The volatilization of these groups causes an improvement in the textural features of the biochars compared to their precursors, being favorable for adsorption purposes.

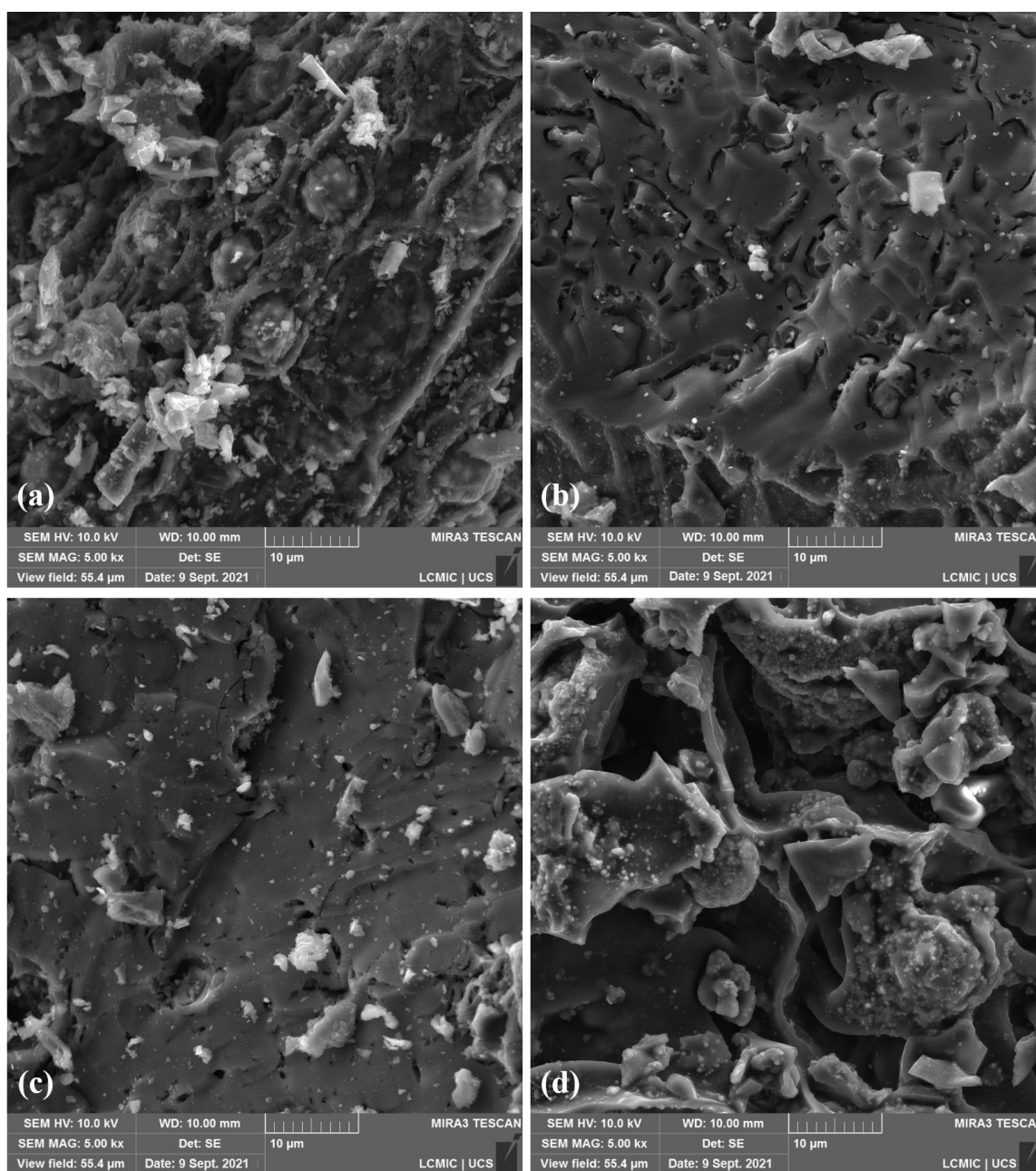
XRD analyzed the biochars of butiá precursors, and the diffraction patterns are shown in the Supplementary Material (Figure S5). No crystalline phase was observed for all biochars, indicating an amorphous structure. This non-regular structure is generally adequate for adsorption purposes [111] since it provides more empty spaces and allows the accommodation of molecules at the solid surface.

Figure 4 shows the micrographs of biochars. These micrographs show cavities that can indicate a thermal degradation reaction during the pyrolysis process, releasing volatile matter and resulting in a visible porous surface, which was later confirmed through pore distribution analysis. In addition, these SEM micrographs confirm that pyrolysis provides modifications into butiá precursors and shows bumps, cavities, and grooves that are favorable for adsorption purposes [99].

$\text{N}_2$  sorption/desorption analysis was performed, and the isotherms are presented in Figure S6 (Supplementary Material). The BET and BJH results are presented in Table 2. From Figure S6 (Supplementary Material), it can be seen that samples FIB.700 (a) and DOA.700 (d) presented type I isotherm, characteristic of solids with microporosity [112]. Nonetheless, Table 2 shows that these biochars have an average pore size slightly higher than 2 nm, the limit for micropores [113]. This range of pore diameter is called narrow mesopores (<2.5 nm) [114] and also presents type I isotherms. Pore size distribution (Figure S7—Supplementary Material) confirms that FIB.700 (a) and DOA.700 (d) presented narrow mesopores. FIB.700 and END.700 (Figure S6a,c) presented non-reversible isotherms attributed to these materials' intrinsic and typical characteristics. Isotherms shapes in Figure S6 are usual for chars and may be explained by the presence of necks. Better results obtained for biochars from FIB and DOA may be explained by the lowest lignin content, already presented in Table 1. Lignin may inhibit porosity [115], resulting in dense solids. These results are similar to those obtained by El-Gamal et al. (2017) [46] for biochars obtained from sugarcane bagasse (0.11  $\text{cm}^3 \text{g}^{-1}$  and 2.31 nm). Additionally, higher cellulose contents may result in a microporous structure formation [51,116,117]. This statement explains the higher pore volume presented by DOA.700, which has more than 50% of cellulose content. The isotherms observed for ALM.700 and END.700 are type IV and II, respectively. These isotherm shapes are characteristic of non-porous solids or relatively higher pores [112]. END.700 and ALM.700 presented the larger pores and the lowest total pore volumes according to isotherm types (Table 2).

**Table 2.** Textural characteristics of the butiá-based biochars.

Sample	Surface Area BET ( $\text{m}^2 \text{g}^{-1}$ )	Average Pore Size (nm)	Micropores Volume ( $\text{cm}^3 \text{g}^{-1}$ )	Mesopores Volume ( $\text{cm}^3 \text{g}^{-1}$ )	Total Volume Pores ( $\text{cm}^3 \text{g}^{-1}$ )	pH <sub>PCZ</sub>
FIB.700	183.59	2.527	0.109	0.0	0.109	6.52
ALM.700	1.92	5.628	0.0	0.00194	0.00194	7.20
END.700	58.39	3.336	0.065	0.0	0.065	7.34
DOA.700	220.43	2.456	0.123	0.0	0.123	7.05



**Figure 4.** SEM micrographs of (a) FIB.700, (b) ALM.700, (c) END.700 and (d) DOA.700.

The highest values for the specific surface area were from FIB.700 and DOA.700 biochars, reaching  $183.59$  and  $220.43 \text{ m}^2 \text{ g}^{-1}$ , respectively. These surface area values are higher than chars modified or activated chars from date stone ( $187 \text{ m}^2 \text{ g}^{-1}$ ) [118], beer solid wastes ( $80.5 \text{ m}^2 \text{ g}^{-1}$ ) [100], corn stover ( $24\text{--}129 \text{ m}^2 \text{ g}^{-1}$ ) [119], and freshwater sludge ( $96\text{--}285.78 \text{ m}^2 \text{ g}^{-1}$ ) [120]. Sample ALM.700 (Table 2) resulted in a lower surface area value. However, the literature reports similar values for other biochars obtained from different materials such as sweet lime ( $1.9 \text{ m}^2 \text{ g}^{-1}$ ) [121], oak bark ( $1.9 \text{ m}^2 \text{ g}^{-1}$ ) [122], and chicken manure wastes ( $0.98\text{--}4.9 \text{ m}^2 \text{ g}^{-1}$ ) [56]. Li et al. (2005) [123] presented that specific surface areas of your biochars ranged from  $65$  to  $95 \text{ m}^2 \text{ g}^{-1}$ . Considering this information, END.700 is also in the literature range. Comparing results obtained for surface area for ALM.700 and DOA.700 (Table 2), the previous oil extraction allows the use for other purposes, which increases the waste's added value and results in better properties for the biochar to act as an adsorbent.

### 2.5. Results of CO<sub>2</sub> Capture on the Biochars

The CO<sub>2</sub> adsorption capacity of biochars was tested at 25 °C and atmospheric pressure. The results are shown in Figure 5. END.700 presented a higher adsorption capacity (66.43 mg g<sup>-1</sup>), and the total adsorption capacity was reached practically in the first minute of the run (58.65 mg g<sup>-1</sup>) with an increase of 11.7%, from 1 to 11.8 min. Botomé et al. (2017) [124] obtained similar capacity and behavior by employing activated carbon from CCA-treated wood to adsorb CO<sub>2</sub> at the same pressure and temperature. It is known that a high surface area and pore volume are needed to improve CO<sub>2</sub> adsorption [125], and this process is dominated by micropores [31]. In parallel, at pyrolysis, the higher lignin content inhibits pore formation [115], and the END precursor has the higher lignin content (Table 1). Consequently, END.700 biochar has a low micropores volume (Table 2). Although micropore volume and surface area are important to CO<sub>2</sub> adsorption, alkalinity strongly influences this process [31]. Table 2 presents the results for pH<sub>PCZ</sub>. END.700 shows the highest value (7.34) at the point of zero charges [126]. This observation may explain why END.700 presented a higher capture than other biochars. CO<sub>2</sub> is a weak Lewis acid gas, which can interact with the alkaline adsorbent, and lignin is a Lewis base. Thus, the higher content of lignin may explain the increase in CO<sub>2</sub> capture. The pH<sub>PCZ</sub> seems to play a secondary role in CO<sub>2</sub> adsorption, Wjihi et al. (2021) [127] reported that a higher pH<sub>PCZ</sub> resulted in higher adsorption capacity. FIB.700 showed an adsorption capacity of 54.59 mg g<sup>-1</sup>, ALM.700 presented 48.87 mg g<sup>-1</sup>, and DOA.700 exhibited an adsorption capacity of 51.76 mg g<sup>-1</sup>, respectively (Figure 6).

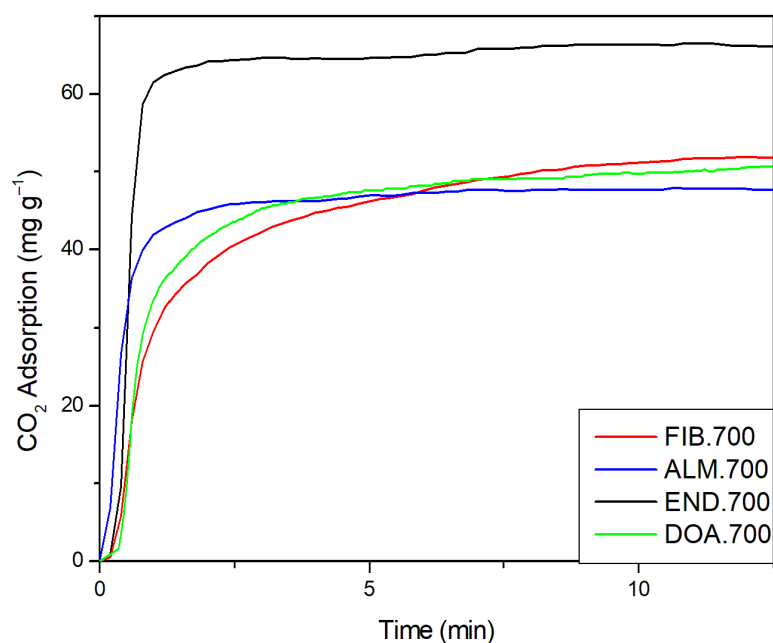


**Figure 5.** CO<sub>2</sub> adsorption capacity of biochars from FIB, ALM, END, and DOA.

Considering that surface area impacts CO<sub>2</sub> adsorption [128], this result can be evaluated in terms of CO<sub>2</sub> mass per unit of area of adsorbent (mg CO<sub>2</sub> m<sup>-2</sup>) [124] bo. The best performance (per unit of area) was reached by ALM.700, which presented an adsorption capacity of 25.45 mg CO<sub>2</sub> m<sup>-2</sup>, higher than marine shale with 14.948 mg CO<sub>2</sub> m<sup>-2</sup> [129]. Table S1 (Supplementary Material) presents a compilation datum of adsorbents from literature to compare with biochars obtained in this work. As can be seen, the biochars produced from butiá precursors pyrolysis without the activation step resulted in a better performance than some activated carbons with large surface area and activation.

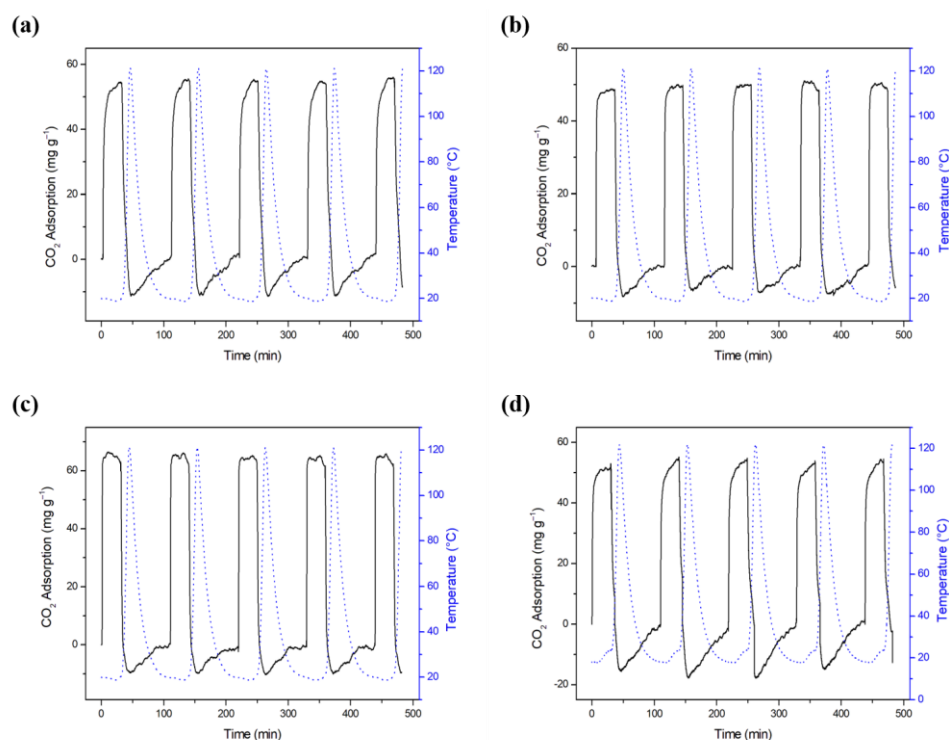


**Figure 6.** CO<sub>2</sub> adsorption cycles in biochars (a) FIB.700, (b) ALM.700, (c) END.700 and (d) DOA.700.

Figure 6 shows the cycles of CO<sub>2</sub> adsorption/desorption for biochars obtained from butiá precursors. The biochars presented fast adsorption and desorption, which is an important feature in selecting an adsorbent. Biochars presented suitable stability for adsorption and desorption cycles, evaluated by the same behavior in the 5 cycles, similar to those presented by Botomé et al. (2017) and Singh et al. (2019) [124,130]. At the first peak, END.700 (Figure 6c) presented 66.43 mg g<sup>-1</sup>. This biochar presented an average capacity of 65.41 mg g<sup>-1</sup>, considering the five peaks, representing a regeneration of 98.5%. The five peaks of FIB.700 (Figure 6a), ALM.700 (Figure 6b) and DOA.700 (Figure 6d) exhibited average capacity of 54.86 ± 0.63 mg g<sup>-1</sup>, 49.91 ± 0.78 mg g<sup>-1</sup> and 52.83 ± 1.02 mg g<sup>-1</sup>, respectively, and regeneration of 100%. Total regeneration for CO<sub>2</sub> adsorbents is also reported by Botomé et al. (2017) and Li and Xiao (2019) [124,131].

### 3. Material and Methods

#### 3.1. Obtainment and Pre-Treatment of the Precursors

The butiá wastes used in this work were donated by familiar agroindustry (Sete de Setembro city, Rio Grande do Sul, Brazil (−28°12′30.7″, −54°29′31.7″)). The pomace was collected after a pulp extractor and was dried in an oven (SP-100/216, SPLabor, Brazil) at 60 °C for 48 h. The dried biomass was separated into fibers and seeds. The seeds were broken to remove the almonds. Fibers (FIB), endocarps (END), and almonds (ALM) were fragmented in a knife mill (DeLeo 0416, Porto Alegre, Brazil) for particle sizes less than 2 mm. Some almonds were separated to extract lipids by Soxhlet in two steps, according to TAPPI, 1997 [132]: firstly, using hexane (Cinética, Brazil) (30 g of almonds to 300 mL of solvent) for 5 h. After, the solids were dried in an oven for solvent removal. The second extraction step was conducted with a mixture of ethanol (Audaz, Brazil) and benzene (Cinética, Brazil) (1:2, *v/v*) for 5 h. Finally, solvents were recovered using a rotary evaporator. The solids obtained after extractions correspond to a deoiled almond (DOA) precursor.

### 3.2. Characterization of the Precursors

The four precursors (FIB, END, ALM, and DOA) were characterized using proximate analysis based on the D3172-89 (1993) standard from the American Society for Testing and Materials [133]. Van Soest's gravimetric method determined the cellulose, hemicellulose, and lignin composition [134]. Fourier transform infrared spectroscopy analysis (Shimadzu, Prestige 21, Japan) was performed to identify functional groups from 4500 to 400  $\text{cm}^{-1}$ . X-ray diffraction (Rigaku, Miniflex 300, Shibuya, Japan) was used to analyze the crystalline or amorphous nature of the samples, applying a Cu K $\alpha$  radiation ( $\lambda = 154,051 \text{ \AA}$ ) at 20 mA and 30 kV by scanning from 5 to 70°, with a step of 0.03°. The thermal stability of the samples was analyzed by Thermogravimetric analysis (STA 449 F3, Jupiter, Netzsch, Selb, Germany) with 10 mg of sample, a heating rate of 5  $^{\circ}\text{C min}^{-1}$  from ambient temperature to 800  $^{\circ}\text{C}$  and nitrogen flow (50  $\text{mL min}^{-1}$ ). The morphology was analyzed by Scanning electron microscopy (Tescan Mira 3, Kohoutovice, Czech Republic), using 5 kV.

### 3.3. Pyrolysis Process

The pyrolysis of FIB, END, ALM, and DOA was performed in a tubular reactor described and reported by Perondi et al. (2017) [34]. The experiments were conducted at a 5  $^{\circ}\text{C min}^{-1}$  heating rate until 700  $^{\circ}\text{C}$ , at 200  $\text{mL min}^{-1}$   $\text{N}_2$  flow, for 100 g of precursor (FIB, END, ALM, or DOA). A 60 min holding time was used after the final temperature (700  $^{\circ}\text{C}$ ) was reached. The gas samples were collected in a non-isothermal region (500, 600, and 700  $^{\circ}\text{C}$  points) and an isothermal region (after 30 and 60 min after 700  $^{\circ}\text{C}$  was reached). The pyrolysis parameters were selected considering previous studies [124] for better biochar and  $\text{H}_2$  generation. The gases and vapors sampling was conducted, as reported by Perondi et al. (2017) [34]. A gas meter was used to measure the volume of gas produced. The bio-oil at boilers and the biochar (residual solid) were collected, and their masses were determined for yield computation. The percentage yields of biochar ( $R_{\text{biochar}}$ ), pyrolytic liquid ( $R_{\text{liquid}}$ ), and non-condensed gases ( $R_{\text{gas}}$ ) were determined as follows:

$$R_{\text{biochar}}(\%) = \frac{m_{\text{biochar}}}{m} \times 100 \quad (1)$$

$$R_{\text{liquid}}(\%) = \frac{m_{\text{liquid}}}{m} \times 100 \quad (2)$$

$$R_{\text{gas}}(\%) = 100 - R_{\text{liquid}} - R_{\text{biochar}} \quad (3)$$

where  $m$  (g) is the mass of precursor material inserted into the reactor,  $m_{\text{biochar}}$  (g) is the residual solids mass in the reactor after the pyrolysis process, and  $m_{\text{liquid}}$  (g) is the total mass of liquid in the collectors after pyrolysis process.

### 3.4. Non-Condensable Gases Characterization

The non-condensable gases ( $\text{H}_2/\text{CO}/\text{CO}_2/\text{CH}_4$ ) analysis was performed by a gas chromatograph (Dani Master GC) equipped with a thermal conductivity detector. A capillary column Carboxen<sup>TM</sup> model 1006 (SUPELCO), with a length of 30 m, 0.53 mm internal diameter, and 30 mm film thickness, was used. The calibration curves were constructed from gas standards.

### 3.5. Biochars Characterization

Solid fractions obtained by pyrolysis of FIB, ALM, END, and DOA were named FIB.700, ALM.700, END.700, and DOA.700, respectively. These biochars were characterized by FTIR, XRD, and SEM, using the same procedure reported in Section 2.2. The  $\text{N}_2$  adsorption-desorption isotherms at  $-196 \text{ }^{\circ}\text{C}$  were obtained in a surface area and porosimetry analyzer (Quantachrome Instruments, Nova 1200) by degassing biochars for 20 h under a vacuum. The surface area was determined by Brunauer Emmett-Teller (BET). The total pore volume was determined from the amount of nitrogen adsorbed at  $P/P_0 = 0.99$ . The micropore area and the micropore volume were estimated by t-plot.  $\text{N}_2$  isotherms and non-local density

functional theory (NLDFT) determined the pore size distribution. The point of zero charges ( $\text{pH}_{\text{PZC}}$ ) was determined by the eleven points experiment as follows: Eleven flasks with 50 mL of a solution containing 50 mg of the samples (initial pH values in the range from 1.0 to 11.0, which were adjusted with HCl and NaOH) were stirred at 120 rpm (Fanem, 315 SE, São Paulo, Brazil) for 24 h. The pH values were measured before and after the agitation (Marte, MB10, São Paulo, Brazil).

### 3.6. Biochars Potential for CO<sub>2</sub> Capture

The biochars FIB.700, END.700, ALM.700, and DOA.700 were used in adsorption to capture CO<sub>2</sub>. CO<sub>2</sub> adsorption studies were carried out in thermogravimetric equipment (Netzsch, STA 449 F3, Jupiter, Selb, Germany), employing 10 mg of biochar, with the same methodology reported by Botomé et al. (2017) [124]. When the point of adsorbent saturation was achieved, CO<sub>2</sub> flow was interrupted, and the sample was heated until 120 °C, under N<sub>2</sub> flow, to desorption. The procedure was repeated until complete five cycles of adsorption–desorption.

## 4. Conclusions

A possible route to valorize butiá wastes was studied in this work. The butiá wastes were divided into fibers, endocarps, almonds, and deoiled almonds, and these fractions were pyrolyzed. The pyrolysis yields varied according to the precursor type. The high yields in terms of biochar (31.9%wt.), bio-oil (72.2%wt.), and gases (50.5%wt.) were found, respectively, for endocarp, almonds and deoiled almonds as precursors. The main gas released was H<sub>2</sub>, regardless of the precursor type. The generated biochars presented interesting features to CO<sub>2</sub> capture (66.43 mg g<sup>-1</sup> or 25.45 mg CO<sub>2</sub> m<sup>-2</sup>), and these characteristics were maintained for 5 cycles. From the cleaner production perspective, the pyrolysis of butiá agro-industrial wastes presented interesting possibilities: power generation by gases and oil released at the process; aggregate value to precursors through the biochar preparation, contributing to solid wastes management, and CO<sub>2</sub> capture by the produced biochar.

**Supplementary Materials:** The following supporting information can be downloaded at: <https://www.mdpi.com/article/10.3390/molecules27217515/s1>, Figure S1: FTIR vibration spectra of butiá precursors; Figure S2: XRD patterns of butiá precursors; Figure S3: SEM micrographs of butiá precursors; Figure S4: FTIR vibrational spectra of biochars; Figure S5: XRD patterns of biochars; Figure S6: N<sub>2</sub> sorption/desorption isotherms of biochars; Figure S7 Pore size distribution of biochars; Table S1 Surface area, CO<sub>2</sub> adsorption capacity and activation agent form different adsorbents presented in literature. References [135–152] are cited in the supplementary materials.

**Author Contributions:** Conceptualization, I.d.S.N., D.P., M.G. and G.L.D.; methodology, D.P. and I.d.S.N.; software, I.d.S.N.; formal analysis, I.d.S.N., M.G., D.P. and G.L.D.; investigation, D.P., J.C.D., L.M.M.M. and F.B.D.N.; resources, M.G. and D.P.; data curation, D.P., C.S. and L.F.O.S.; writing—original draft preparation, I.d.S.N. and G.L.D.; writing—review and editing, D.P., M.G., I.d.S.N. and G.L.D.; visualization, M.G.; supervision, G.L.D.; project administration, D.P. and G.L.D.; funding acquisition, G.L.D. All authors have read and agreed to the published version of the manuscript.

**Funding:** This research received no external funding.

**Institutional Review Board Statement:** Not applicable.

**Informed Consent Statement:** Not applicable.

**Data Availability Statement:** Data available upon reasonable request.

**Conflicts of Interest:** The authors declare no conflict of interest.

**Sample Availability:** Samples of the compounds are not available from the authors.

## References

1. Ibrahim, M.; Vo, X.V. Exploring the Relationships among Innovation, Financial Sector Development and Environmental Pollution in Selected Industrialized Countries. *J. Environ. Manage.* **2021**, *284*, 112057. [[CrossRef](#)] [[PubMed](#)]
2. Ma, X.; Wu, Y.; Fang, M.; Liu, B.; Chen, R.; Shi, R.; Wu, Q.; Zeng, Z.; Li, L. In-Situ Activated Ultramicroporous Carbon Materials Derived from Waste Biomass for CO<sub>2</sub> Capture and Benzene Adsorption. *Biomass Bioenergy* **2022**, *158*, 106353. [[CrossRef](#)]
3. Bergstra, A.D.; Brunekreef, B.; Burdorf, A. The Influence of Industry-Related Air Pollution on Birth Outcomes in an Industrialized Area. *Environ. Pollut.* **2021**, *269*, 115741. [[CrossRef](#)]
4. Bernstein, A.S.; Rice, M.B. Lungs in a Warming World: Climate Change and Respiratory Health. *Chest* **2013**, *143*, 1455–1459. [[CrossRef](#)]
5. Horemans, J.A.; Janssens, I.A.; Gielen, B.; Roland, M.; Deckmyn, G.; Verstraeten, A.; Neiryneck, J.; Ceulemans, R. Weather, Pollution and Biotic Factors Drive Net Forest—Atmosphere Exchange of CO<sub>2</sub> at Different Temporal Scales in a Temperate-Zone Mixed Forest. *Agric. For. Meteorol.* **2020**, *291*, 108059. [[CrossRef](#)]
6. Lelandais, L.; Xueref-Remy, I.; Riandet, A.; Blanc, P.E.; Armengaud, A.; Oppo, S.; Yohia, C.; Ramonet, M.; Delmotte, M. Analysis of 5.5 Years of Atmospheric CO<sub>2</sub>, CH<sub>4</sub>, CO Continuous Observations (2014–2020) and Their Correlations, at the Observatoire de Haute Provence, a Station of the ICOS-France National Greenhouse Gases Observation Network. *Atmos. Environ.* **2022**, *277*, 119020. [[CrossRef](#)]
7. Bao, J.; Lu, W.H.; Zhao, J.; Bi, X.T. Greenhouses for CO<sub>2</sub> Sequestration from Atmosphere. *Carbon Resour. Convers.* **2018**, *1*, 183–190. [[CrossRef](#)]
8. Khalidy, R.; Santos, R.M. The Fate of Atmospheric Carbon Sequestered through Weathering in Mine Tailings. *Miner. Eng.* **2021**, *163*, 106767. [[CrossRef](#)]
9. Breuer, J.L.; Samsun, R.C.; Stolten, D.; Peters, R. How to Reduce the Greenhouse Gas Emissions and Air Pollution Caused by Light and Heavy Duty Vehicles with Battery-Electric, Fuel Cell-Electric and Catenary Trucks. *Environ. Int.* **2021**, *152*, 106474. [[CrossRef](#)]
10. Zhang, Y.; Zhu, C.; Chu, C.; Fu, T.; Ma, Y. Mass Transfer and Capture of Carbon Dioxide Using Amino Acids Sodium Aqueous Solution in Microchannel. *Chem. Eng. Process.—Process Intensif.* **2022**, *173*, 108831. [[CrossRef](#)]
11. Nasrifar, K.; Moshfeghian, M. Thermodynamics of Carbon Dioxide Mixtures at Cryogenic Conditions. *Cryogenics* **2022**, *121*, 103404. [[CrossRef](#)]
12. Singh, S.; Varghese, A.M.; Reinalda, D.; Karanikolos, G.N. Graphene—Based Membranes for Carbon Dioxide Separation. *J. CO<sub>2</sub> Util.* **2021**, *49*, 101544. [[CrossRef](#)]
13. Pu, Q.; Zou, J.; Wang, J.; Lu, S.; Ning, P.; Huang, L.; Wang, Q. Systematic Study of Dynamic CO<sub>2</sub> Adsorption on Activated Carbons Derived from Different Biomass. *J. Alloys Compd.* **2021**, *887*, 161406. [[CrossRef](#)]
14. Pires, J.; Jużków, J.; Pinto, M.L. Amino Acid Modified Montmorillonite Clays as Sustainable Materials for Carbon Dioxide Adsorption and Separation. *Colloids Surf. A Physicochem. Eng. Asp.* **2018**, *544*, 105–110. [[CrossRef](#)]
15. Surra, E.; Ribeiro, R.P.P.L.; Santos, T.; Bernardo, M.; Mota, J.P.B.; Lapa, N.; Esteves, I.A.A.C. Evaluation of Activated Carbons Produced from Maize Cob Waste for Adsorption-Based CO<sub>2</sub> Separation and Biogas Upgrading. *J. Environ. Chem. Eng.* **2022**, *10*, 107065. [[CrossRef](#)]
16. Chen, J.; Jiang, L.; Wang, W.; Shen, Z.; Liu, S.; Li, X.; Wang, Y. Constructing Highly Porous Carbon Materials from Porous Organic Polymers for Superior CO<sub>2</sub> Adsorption and Separation. *J. Colloid Interface Sci.* **2022**, *609*, 775–784. [[CrossRef](#)]
17. An, X.; Zhao, K.; Zhang, W.; Yang, J.; Liao, Y.; Wang, L.; Fu, D. Tailoring the Pore Structure Modified with Functional Groups for Superior CO<sub>2</sub> Adsorption Capacity and the Selectivity of Separation. *Fuel* **2022**, *309*, 122175. [[CrossRef](#)]
18. Zhang, X.; Zhang, S.; Yang, H.; Feng, Y.; Chen, Y.; Wang, X.; Chen, H. Nitrogen Enriched Biochar Modified by High Temperature CO<sub>2</sub>-Ammonia Treatment: Characterization and Adsorption of CO<sub>2</sub>. *Chem. Eng. J.* **2014**, *257*, 20–27. [[CrossRef](#)]
19. Li, S.; Yuan, X.; Deng, S.; Zhao, L.; Lee, K.B. A Review on Biomass-Derived CO<sub>2</sub> Adsorption Capture: Adsorbent, Adsorber, Adsorption, and Advice. *Renew. Sustain. Energy Rev.* **2021**, *152*, 111708. [[CrossRef](#)]
20. Goel, C.; Mohan, S.; Dinesha, P. CO<sub>2</sub> Capture by Adsorption on Biomass-Derived Activated Char: A Review. *Sci. Total Environ.* **2021**, *798*, 149296. [[CrossRef](#)]
21. Hussin, F.; Aroua, M.K.; Yusoff, R. Adsorption of CO<sub>2</sub> on Palm Shell Based Activated Carbon Modified by Deep Eutectic Solvent: Breakthrough Adsorption Study. *J. Environ. Chem. Eng.* **2021**, *9*, 105333. [[CrossRef](#)]
22. Bhatta, L.K.G.; Venkatesh, K.; N, K.; Gundanna, S.K.; Bhatta, U.M. Synthesis and Characterization of Activated Carbon from Delonix Regia Seeds for CO<sub>2</sub> Adsorption. *Energy Clim. Chang.* **2021**, *2*, 100064. [[CrossRef](#)]
23. Mochizuki, Y.; Bud, J.; Byambajav, E.; Tsubouchi, N. Influence of Ammonia Treatment on the CO<sub>2</sub> Adsorption of Activated Carbon. *J. Environ. Chem. Eng.* **2022**, *10*, 107273. [[CrossRef](#)]
24. Nazir, G.; Rehman, A.; Park, S.J. Valorization of Shrimp Shell Biowaste for Environmental Remediation: Efficient Contender for CO<sub>2</sub> Adsorption and Separation. *J. Environ. Manage.* **2021**, *299*, 113661. [[CrossRef](#)]
25. Li, J.; Bao, A.; Chen, J.; Bao, Y. A Green Route to CO<sub>2</sub> Adsorption on Biomass Chitosan Derived Nitrogen-Doped Micropore-Dominated Carbon Nanosheets by Different Activators. *J. Environ. Chem. Eng.* **2022**, *10*, 107021. [[CrossRef](#)]
26. Kim, M.; Lee, J.W.; Kim, S.; Kang, Y.T. CO<sub>2</sub> Adsorption on Zeolite 13X Modified with Hydrophobic Octadecyltrimethoxysilane for Indoor Application. *J. Clean. Prod.* **2022**, *337*, 130597. [[CrossRef](#)]

27. Gan, F.; Wang, B.; Jin, Z.; Xie, L.; Dai, Z.; Zhou, T.; Jiang, X. From Typical Silicon-Rich Biomass to Porous Carbon-Zeolite Composite: A Sustainable Approach for Efficient Adsorption of CO<sub>2</sub>. *Sci. Total Environ.* **2021**, *768*, 144529. [[CrossRef](#)]
28. Aquatar, M.O.; Bhatia, U.; Rayalu, S.S.; Krupadam, R.J. Reduced Graphene Oxide -MnO<sub>2</sub> Nanocomposite for CO<sub>2</sub> Capture from Flue Gases at Elevated Temperatures. *Sci. Total Environ.* **2022**, *816*, 151522. [[CrossRef](#)]
29. Ghanbari, T.; Abnisa, F.; Wan Daud, W.M.A. A Review on Production of Metal Organic Frameworks (MOF) for CO<sub>2</sub> Adsorption. *Sci. Total Environ.* **2020**, *707*, 135090. [[CrossRef](#)]
30. Daud, N.K.; Najib, N.H.I.M. Adsorption of CO<sub>2</sub> on ZSM-5 and Cu-MOF at Room Temperature and Low Pressure Conditions for Carbon Capture and Storage (CCS) Application. *Mater. Today Proc.* **2022**, *57*, 1345–1355. [[CrossRef](#)]
31. Cao, L.; Zhang, X.; Xu, Y.; Xiang, W.; Wang, R.; Ding, F.; Hong, P.; Gao, B. Straw and Wood Based Biochar for CO<sub>2</sub> Capture: Adsorption Performance and Governing Mechanisms. *Sep. Purif. Technol.* **2022**, *287*, 120592. [[CrossRef](#)]
32. Lampropoulos, A.; Kaklidis, N.; Athanasiou, C.; Montes-Morán, M.A.; Arenillas, A.; Menéndez, J.A.; Binas, V.D.; Konsolakis, M.; Marnellos, G.E. Effect of Olive Kernel Thermal Treatment (Torrefaction vs. Slow Pyrolysis) on the Physicochemical Characteristics and the CO<sub>2</sub> or H<sub>2</sub>O Gasification Performance of as-Prepared Biochars. *Int. J. Hydrogen Energy* **2021**, *46*, 29126–29141. [[CrossRef](#)]
33. Xie, W.-H.; Li, H.; Yang, M.; He, L.-N.; Li, H.-R. CO<sub>2</sub> Capture and Utilization with Solid Waste. *Green Chem. Eng.* **2022**, *3*, 199–209. [[CrossRef](#)]
34. Perondi, D.; Poletto, P.; Restelatto, D.; Manera, C.; Silva, J.P.; Junges, J.; Collazzo, G.C.; Dettmer, A.; Godinho, M.; Vilela, A.C.F. Steam Gasification of Poultry Litter Biochar for Bio-Syngas Production. *Process Saf. Environ. Prot.* **2017**, *109*, 478–488. [[CrossRef](#)]
35. Li, Z.; Xing, B.; Ding, Y.; Li, Y.; Wang, S. A High-Performance Biochar Produced from Bamboo Pyrolysis with in-Situ Nitrogen Doping and Activation for Adsorption of Phenol and Methylene Blue. *Chinese J. Chem. Eng.* **2020**, *28*, 2872–2880. [[CrossRef](#)]
36. Lawal, A.A.; Hassan, M.A.; Ahmad Farid, M.A.; Tengku Yasim-Anuar, T.A.; Samsudin, M.H.; Mohd Yusoff, M.Z.; Zakaria, M.R.; Mokhtar, M.N.; Shirai, Y. Adsorption Mechanism and Effectiveness of Phenol and Tannic Acid Removal by Biochar Produced from Oil Palm Frond Using Steam Pyrolysis. *Environ. Pollut.* **2021**, *269*, 116197. [[CrossRef](#)]
37. Karimi, M.; Shirzad, M.; Silva, J.A.C.; Rodrigues, A.E. Biomass/Biochar Carbon Materials for CO<sub>2</sub> Capture and Sequestration by Cyclic Adsorption Processes: A Review and Prospects for Future Directions. *J. CO<sub>2</sub> Util.* **2022**, *57*, 101890. [[CrossRef](#)]
38. Shafawi, A.N.; Mohamed, A.R.; Lahijani, P.; Mohammadi, M. Recent Advances in Developing Engineered Biochar for CO<sub>2</sub> Capture: An Insight into the Biochar Modification Approaches. *J. Environ. Chem. Eng.* **2021**, *9*, 106869. [[CrossRef](#)]
39. Cuong, D.V.; Matsagar, B.M.; Lee, M.; Hossain, M.S.A.; Yamauchi, Y.; Vithanage, M.; Sarkar, B.; Ok, Y.S.; Wu, K.C.W.; Hou, C.H. A Critical Review on Biochar-Based Engineered Hierarchical Porous Carbon for Capacitive Charge Storage. *Renew. Sustain. Energy Rev.* **2021**, *145*, 111029. [[CrossRef](#)]
40. Wan, J.; Liu, L.; Ayub, K.S.; Zhang, W.; Shen, G.; Hu, S.; Qian, X. Characterization and Adsorption Performance of Biochars Derived from Three Key Biomass Constituents. *Fuel* **2020**, *269*, 117142. [[CrossRef](#)]
41. Amin, M.T.; Alazba, A.A.; Shafiq, M. Removal of Copper and Lead Using Banana Biochar in Batch Adsorption Systems: Isotherms and Kinetic Studies. *Arab. J. Sci. Eng.* **2018**, *43*, 5711–5722. [[CrossRef](#)]
42. Gallo-Cordova, A.; Silva-Gordillo, M.D.M.; Muñoz, G.A.; Arboleda-Faini, X.; Almeida Streitwieser, D. Comparison of the Adsorption Capacity of Organic Compounds Present in Produced Water with Commercially Obtained Walnut Shell and Residual Biomass. *J. Environ. Chem. Eng.* **2017**, *5*, 4041–4050. [[CrossRef](#)]
43. Hao, Z.; Wang, C.; Yan, Z.; Jiang, H.; Xu, H. Magnetic Particles Modification of Coconut Shell-Derived Activated Carbon and Biochar for Effective Removal of Phenol from Water. *Chemosphere* **2018**, *211*, 962–969. [[CrossRef](#)] [[PubMed](#)]
44. Georjin, J.; da Boit Martinello, K.; Franco, D.S.P.; Netto, M.S.; Piccilli, D.G.A.; Yilmaz, M.; Silva, L.F.O.; Dotto, G.L. Residual Peel of Pitaya Fruit (*Hylocereus Undatus*) as a Precursor to Obtaining an Efficient Carbon-Based Adsorbent for the Removal of Metanil Yellow Dye from Water. *J. Environ. Chem. Eng.* **2022**, *10*, 107006. [[CrossRef](#)]
45. Lang, J.; Matějová, L.; Cuentas-Gallegos, A.K.; Lobato-Peralta, D.R.; Ainassaari, K.; Gómez, M.M.; Solís, J.L.; Mondal, D.; Keiski, R.L.; Cruz, G.J.F. Evaluation and Selection of Biochars and Hydrochars Derived from Agricultural Wastes for the Use as Adsorbent and Energy Storage Materials. *J. Environ. Chem. Eng.* **2021**, *9*, 105979. [[CrossRef](#)]
46. El-gamal, E.H.; Saleh, M.; Elsokkary, I.; Rashad, M.; El-latif, M.M.A. Comparison between Properties of Biochar Produced by Traditional and Controlled Pyrolysis Comparison between Properties of Biochar Produced by Traditional and Controlled Pyrolysis. *Alex. Sci. Exch. J.* **2017**, *38*, 412–425.
47. Tomul, F.; Arslan, Y.; Kabak, B.; Trak, D.; Kendüzler, E.; Lima, E.C.; Tran, H.N. Peanut Shells-Derived Biochars Prepared from Different Carbonization Processes: Comparison of Characterization and Mechanism of Naproxen Adsorption in Water. *Sci. Total Environ.* **2020**, *726*, 137828. [[CrossRef](#)]
48. Zhang, S.; Ji, Y.; Dang, J.; Zhao, J.; Chen, S. Magnetic Apple Pomace Biochar: Simple Preparation, Characterization, and Application for Enriching Ag(I) in Effluents. *Sci. Total Environ.* **2019**, *668*, 115–123. [[CrossRef](#)]
49. Mohammed, N.A.S.; Abu-Zurayk, R.A.; Hamadneh, I.; Al-Dujaili, A.H. Phenol Adsorption on Biochar Prepared from the Pine Fruit Shells: Equilibrium, Kinetic and Thermodynamics Studies. *J. Environ. Manag.* **2018**, *226*, 377–385. [[CrossRef](#)]
50. Obey, G.; Adelaide, M.; Ramaraj, R. Biochar Derived from Non-Customized Matamba Fruit Shell as an Adsorbent for Wastewater Treatment. *J. Bioresour. Bioprod.* **2022**, *7*, 109–115. [[CrossRef](#)]
51. Lawal, A.A.; Hassan, M.A.; Zakaria, M.R.; Yusoff, M.Z.M.; Norrrahim, M.N.F.; Mokhtar, M.N.; Shirai, Y. Effect of Oil Palm Biomass Cellulosic Content on Nanopore Structure and Adsorption Capacity of Biochar. *Bioresour. Technol.* **2021**, *332*, 125070. [[CrossRef](#)] [[PubMed](#)]

52. Albalasmeh, A.; Gharaibeh, M.A.; Mohawesh, O.; Alajlouni, M.; Quzaih, M.; Masad, M.; El Hanandeh, A. Characterization and Artificial Neural Networks Modelling of Methylene Blue Adsorption of Biochar Derived from Agricultural Residues: Effect of Biomass Type, Pyrolysis Temperature, Particle Size. *J. Saudi Chem. Soc.* **2020**, *24*, 811–823. [[CrossRef](#)]
53. Giri, D.D.; Jha, J.M.; Srivastava, N.; Hashem, A.; Abd\_Allah, E.F.; Shah, M.; Pal, D.B. Sustainable Removal of Arsenic from Simulated Wastewater Using Solid Waste Seed Pods Biosorbents of Cassia Fistula L. *Chemosphere* **2022**, *287*, 132308. [[CrossRef](#)] [[PubMed](#)]
54. Streit, A.F.M.; Côrtes, L.N.; Druzian, S.P.; Godinho, M.; Collazzo, G.C.; Perondi, D.; Dotto, G.L. Development of High Quality Activated Carbon from Biological Sludge and Its Application for Dyes Removal from Aqueous Solutions. *Sci. Total Environ.* **2019**, *660*, 277–287. [[CrossRef](#)] [[PubMed](#)]
55. Wu, C.; Fu, L.; Li, H.; Liu, X.; Wan, C. Using Biochar to Strengthen the Removal of Antibiotic Resistance Genes: Performance and Mechanism. *Sci. Total Environ.* **2022**, *816*, 151554. [[CrossRef](#)]
56. Yıldız, Z.; Kaya, N.; Topcu, Y.; Uzun, H. Pyrolysis and Optimization of Chicken Manure Wastes in Fluidized Bed Reactor: CO<sub>2</sub> Capture in Activated Bio-Chars. *Process Saf. Environ. Prot.* **2019**, *130*, 297–305. [[CrossRef](#)]
57. Idrees, M.; Batool, S.; Kalsoom, T.; Yasmeen, S.; Kalsoom, A.; Raina, S.; Zhuang, Q.; Kong, J. Animal Manure-Derived Biochars Produced via Fast Pyrolysis for the Removal of Divalent Copper from Aqueous Media. *J. Environ. Manag.* **2018**, *213*, 109–118. [[CrossRef](#)]
58. Creamer, A.E.; Gao, B. Carbon-Based Adsorbents for Postcombustion CO<sub>2</sub> Capture: A Critical Review. *Environ. Sci. Technol.* **2016**, *50*, 7276–7289. [[CrossRef](#)]
59. Hoffmann, J.F.; Barbieri, R.L.; Rombaldi, C.V.; Chaves, F.C. Butia Spp. (Arecaceae): An Overview. *Sci. Hortic.* **2014**, *179*, 122–131. [[CrossRef](#)]
60. Sosinski, Ê.E.; Urruth, L.M.; Barbieri, R.L.; Marchi, M.M.; Martens, S.G. On the Ecological Recognition of Butia Palm Groves as Integral Ecosystems: Why Do We Need to Widen the Legal Protection and the in Situ/on-Farm Conservation Approaches? *Land Use Policy* **2019**, *81*, 124–130. [[CrossRef](#)]
61. de Jesus Matias Ventura, L.; Pereira, G.S.L.; Mazzottini-dos-Santos, H.C.; de Lima, J.P.; Mercadante-Simões, M.O.; Lopes, P.S.N.; Ribeiro, L.M. Cytological Aspects of Butia Capitata (Arecaceae) Fruit Maturation and Senescence. *Sci. Hortic.* **2022**, *297*, 110938. [[CrossRef](#)]
62. dos Santos Cruxen, C.E.; Hoffmann, J.F.; Zandoná, G.P.; Fiorentini, Â.M.; Rombaldi, C.V.; Chaves, F.C. Probiotic Butiá (Butia Odorata) Ice Cream: Development, Characterization, Stability of Bioactive Compounds, and Viability of Bifidobacterium Lactis during Storage. *LWT* **2017**, *75*, 379–385. [[CrossRef](#)]
63. Camboim Rockett, F.; de Oliveira Schmidt, H.; Schmidt, L.; Rodrigues, E.; Tischer, B.; Ruffo de Oliveira, V.; Lima da Silva, V.; Rossini Augusti, P.; Hickmann Flôres, S.; Rios, A. Phenolic Compounds and Antioxidant Activity in Vitro and in Vivo of Butia and Opuntia Fruits. *Food Res. Int.* **2020**, *137*, 109740. [[CrossRef](#)] [[PubMed](#)]
64. Barbieri, R.L.; Gomes, J.C.C.; Alercia, A.; Padulosi, S. Agricultural Biodiversity in Southern Brazil: Integrating Efforts for Conservation and Use of Neglected and Underutilized Species. *Sustainability* **2014**, *6*, 741–757. [[CrossRef](#)]
65. Haubert, L.; Zehetmeyr, M.L.; Pereira, Y.M.N.; Kroning, I.S.; Maia, D.S.V.; Sehn, C.P.; Lopes, G.V.; de Lima, A.S.; da Silva, W.P. Tolerance to Benzalkonium Chloride and Antimicrobial Activity of Butia Odorata Barb. Rodr. Extract in Salmonella Spp. Isolates from Food and Food Environments. *Food Res. Int.* **2019**, *116*, 652–659. [[CrossRef](#)]
66. Maia, D.S.V.; Haubert, L.; Kroning, I.S.; Soares, K.; dos, S.; Oliveira, T.L.; da Silva, W.P. Biofilm Formation by Staphylococcus Aureus Isolated from Food Poisoning Outbreaks and Effect of Butia Odorata Barb. Rodr. Extract on Planktonic and Biofilm Cells. *LWT* **2020**, *117*, 108685. [[CrossRef](#)]
67. Vieira, B.M.; Elicker, C.; Nunes, C.F.P.; Bairros, A.V.; Becker, E.M.; de Oliveira, D.M.; Piva, E.; Fontoura, L.A.M.; Pereira, C.M.P. The Synthesis and Characterization of Butia Capitata Seed Oil as a FAME Feedstock. *Fuel* **2016**, *184*, 533–535. [[CrossRef](#)]
68. Zanuttini, M.S.; Pisarello, M.L.; Querini, C.A. Butia Yatay Coconut Oil: Process Development for Biodiesel Production and Kinetics of Esterification with Ethanol. *Energy Convers. Manag.* **2014**, *85*, 407–416. [[CrossRef](#)]
69. Peralta, S.L.; de Carvalho, P.H.A.; Ccahuana-Vásquez, R.A.; de Pereira, C.M.P.; Cury, J.A.; Piva, E.; Lund, R.G. Cytotoxicity, Genotoxicity and Antibiofilm Activity on Streptococcus Mutans of an Experimental Self-Etching Adhesive System Containing Natural Butia Capitata Oil. *Int. J. Adhes. Adhes.* **2017**, *78*, 95–101. [[CrossRef](#)]
70. Cruz, P.N.; Pereira, T.C.S.; Guindani, C.; Oliveira, D.A.; Rossi, M.J.; Ferreira, S.R.S. Antioxidant and Antibacterial Potential of Butia (Butia Catarinensis) Seed Extracts Obtained by Supercritical Fluid Extraction. *J. Supercrit. Fluids* **2017**, *119*, 229–237. [[CrossRef](#)]
71. Kerkhoff, C.M.; da Boit Martinello, K.; Franco, D.S.P.; Netto, M.S.; Georgin, J.; Foletto, E.L.; Picilli, D.G.A.; Silva, L.F.O.; Dotto, G.L. Adsorption of Ketoprofen and Paracetamol and Treatment of a Synthetic Mixture by Novel Porous Carbon Derived from Butia Capitata Endocarp. *J. Mol. Liq.* **2021**, *339*, 117184. [[CrossRef](#)]
72. Cunha, M.R.; Lima, E.C.; Lima, D.R.; da Silva, R.S.; Thue, P.S.; Seliem, M.K.; Sher, F.; dos Reis, G.S.; Larsson, S.H. Removal of Captopril Pharmaceutical from Synthetic Pharmaceutical-Industry Wastewaters: Use of Activated Carbon Derived from Butia Catarinensis. *J. Environ. Chem. Eng.* **2020**, *8*, 104506. [[CrossRef](#)]
73. Mishra, R.K. Pyrolysis of Low-Value Waste Switchgrass: Physicochemical Characterization, Kinetic Investigation, and Online Characterization of Hot Pyrolysis Vapours. *Bioresour. Technol.* **2022**, *347*, 126720. [[CrossRef](#)] [[PubMed](#)]

74. Selvarajoo, A.; Oochit, D. Effect of Pyrolysis Temperature on Product Yields of Palm Fibre and Its Biochar Characteristics. *Mater. Sci. Energy Technol.* **2020**, *3*, 575–583. [[CrossRef](#)]
75. de Godois Baroni, É.; Tannous, K.; Rueda-Ordóñez, Y.J.; Tinoco-navarro, L.K. The Applicability of Isoconversional Models in Estimating the Kinetic Parameters of Biomass Pyrolysis. *J. Ther. Anal. Calorim.* **2015**, *123*, 909–917. [[CrossRef](#)]
76. Aygün, A.; Yenisooy-Karakaş, S.; Duman, I. Production of Granular Activated Carbon from Fruit Stones and Nutshells and Evaluation of Their Physical, Chemical and Adsorption Properties. *Microporous Mesoporous Mater.* **2003**, *66*, 189–195. [[CrossRef](#)]
77. Santos, V.O.; Queiroz, L.S.; Araujo, R.O.; Ribeiro, F.C.P.; Guimarães, M.N.; Carlos, E.F.; Chaar, J.S.; De Souza, L.K.C. Pyrolysis of Acai Seed Biomass: Kinetics and Thermodynamic Parameters Using Thermogravimetric Analysis. *Bioresour. Technol. Reports* **2020**, *12*, 100553. [[CrossRef](#)]
78. Ahmad, M.S.; Mehmood, M.A.; Al Ayed, O.S.; Ye, G.; Luo, H.; Ibrahim, M.; Rashid, U.; Arbi Nehdi, I.; Qadir, G. Kinetic Analyses and Pyrolytic Behavior of Para Grass (*Urochloa Mutica*) for Its Bioenergy Potential. *Bioresour. Technol.* **2017**, *224*, 708–713. [[CrossRef](#)]
79. Toribio-cuaya, H.; Pedraza-segura, L.; Macías-bravo, S. Biological and Physical Sciences Characterization of Lignocellulosic Biomass Using Five Simple Steps. *J. Chem. Biol. Phys. Sci.* **2014**, *4*, 28–49.
80. Siqueira, P.; Mabel, M.; Helena, R.; De Oliveira, J.; Prado, A.; Matias, S.; Alencar, D. Açai Seeds: An Unexplored Agro-Industrial Residue as a Potential Source of Lipids, Fibers, and Antioxidant Phenolic Compounds. *Ind. Crops Prod.* **2021**, *161*, 113204.
81. Rasool, T.; Najar, I.; Chandra, V.; Pandey, A. Pyrolysis of Almond (*Prunus Amygdalus*) Shells: Kinetic Analysis, Modelling, Energy Assessment and Technical Feasibility Studies. *Bioresour. Technol.* **2021**, *337*, 125466. [[CrossRef](#)] [[PubMed](#)]
82. Hansted, A.L.S.; Cacuro, T.A.; Nakashima, G.T.; Costa, V.E.; Yamamoto, H.; Yamaji, F.M. Industrial Crops & Products Use of a Lignocellulosic Residue as Solid Fuel: The Effect of Ash Content in the Energy Potential. *Ind. Crops Prod.* **2018**, *116*, 209–214. [[CrossRef](#)]
83. Reshad, A.S.; Tiwari, P.; Goud, V.V. Thermo-Chemical Conversion of Waste Rubber Seed Shell to Produce Fuel and Value-Added Chemicals. *J. Energy Inst.* **2018**, *91*, 940–950. [[CrossRef](#)]
84. Sangaré, D.; Bostyn, S.; Santillán, M.M.; García-Alamilla, P.; Belandria, V.; Gökalp, I. Comparative Pyrolysis Studies of Lignocellulosic Biomasses: Online Gas Quantification, Kinetics Triplets, and Thermodynamic Parameters of the Process. *Bioresour. Technol.* **2022**, *346*, 126598. [[CrossRef](#)] [[PubMed](#)]
85. Rambo, M.K.D.; Alexandre, G.P.; Rambo, M.C.D.; Alves, A.R.; Garcia, W.T.; Baruque, E. Characterization of Biomasses from the North and Northeast Regions of Brazil for Processes in Biorefineries. *Food Sci. Technol.* **2015**, *35*, 605–611. [[CrossRef](#)]
86. Li, S.; Li, J.; Xu, J. Investigating the Release Behavior of Biomass and Coal during the Co-Pyrolysis Process. *Int. J. Hydrog. Energy* **2021**, *46*, 34652–34662. [[CrossRef](#)]
87. Cui, T.; Xu, J.; Fan, W.; Chang, Q.; Yu, G.; Wang, F. Experimental Study on Fragmental Behavior of Coals and Biomasses during Rapid Pyrolysis. *Bioresour. Technol.* **2016**, *222*, 439–447. [[CrossRef](#)]
88. Vasudev, V.; Ku, X.; Lin, J. Kinetic Study and Pyrolysis Characteristics of Algal and Lignocellulosic Biomasses. *Bioresour. Technol.* **2019**, *288*, 121496. [[CrossRef](#)]
89. Sahoo, A.; Kumar, S.; Kumar, J.; Bhaskar, T. A Detailed Assessment of Pyrolysis Kinetics of Invasive Lignocellulosic Biomasses (*Prosopis Juliflora* and *Lantana Camara*) by Thermogravimetric Analysis. *Bioresour. Technol.* **2021**, *319*, 124060. [[CrossRef](#)]
90. Aguiar, M.C.S.; Silvério, F.O.; de Pinho, G.P.; Lopes, P.S.N.; Fidêncio, P.H.; Ventura, S.J. Volatile Compounds from Fruits of *Butia Capitata* at Different Stages of Maturity and Storage. *Food Res. Int.* **2014**, *62*, 1095–1099. [[CrossRef](#)]
91. Kumar, M.; Kumar, S.; Upadhyay, S.N.; Mishra, P.K. Analysis of Thermal Degradation of Banana (*Musa Balbisiana*) Trunk Biomass Waste Using Iso-Conversional Models. *Bioresour. Technol.* **2020**, *310*, 123393. [[CrossRef](#)] [[PubMed](#)]
92. Hernowo, P.; Steven, S.; Restiawaty, E.; Irawan, A.; Borromeus, C.; Marno, S.; Meliana, Y.; Bindar, Y. Chemicals Component Yield Prediction and Kinetic Parameters Determination of Oil Palm Shell Pyrolysis through Volatile State Approach and Experimental Study. *J. Anal. Appl. Pyrolysis* **2022**, *161*, 105399. [[CrossRef](#)]
93. Raza, M.; Abu-jdayil, B.; Al-marzouqi, A.H.; Inayat, A. Kinetic and Thermodynamic Analyses of Date Palm Surface Fibers Pyrolysis Using Coats-Redfern Method. *Renew. Energy* **2022**, *183*, 67–77. [[CrossRef](#)]
94. Cai, J.; He, Y.; Yu, X.; Banks, S.W.; Yang, Y.; Zhang, X.; Yu, Y.; Liu, R.; Bridgwater, A.V. Review of Physicochemical Properties and Analytical Characterization of Lignocellulosic Biomass. *Renew. Sustain. Energy Rev.* **2017**, *76*, 309–322. [[CrossRef](#)]
95. Ma, Z.; Chen, D.; Gu, J.; Bao, B.; Zhang, Q. Determination of Pyrolysis Characteristics and Kinetics of Palm Kernel Shell Using TGA—FTIR and Model-Free Integral Methods. *Energy Convers. Manag.* **2015**, *89*, 251–259. [[CrossRef](#)]
96. Salgado-ramos, M.; Martí-quijal, F.J.; Huertas-alonso, A.J.; Barba, F.J. Almond Hull Biomass: Preliminary Characterization and Development of Two Alternative Valorization Routes by Applying Innovative and Sustainable Technologies. *Ind. Crops Prod.* **2022**, *179*, 114697. [[CrossRef](#)]
97. Yang, H.; Yan, R.; Chen, H.; Lee, D.H.; Zheng, C. Characteristics of Hemicellulose, Cellulose and Lignin Pyrolysis. *Fuel* **2007**, *86*, 1781–1788. [[CrossRef](#)]
98. Poletto, M.; Zattera, A.J.; Forte, M.M.C.; Santana, R.M.C. Thermal Decomposition of Wood: Influence of Wood Components and Cellulose Crystallite Size. *Bioresour. Technol.* **2012**, *109*, 148–153. [[CrossRef](#)]
99. Zazycki, M.A.; Godinho, M.; Perondi, D.; Foletto, E.L.; Collazzo, G.C.; Dotto, G.L. New Biochar from Pecan Nutshells as an Alternative Adsorbent for Removing Reactive Red 141 from Aqueous Solutions. *J. Clean. Prod.* **2018**, *171*, 57–65. [[CrossRef](#)]

100. Franciski, M.A.; Peres, E.C.; Godinho, M.; Perondi, D.; Foletto, E.L.; Collazzo, G.C.; Dotto, G.L. Development of CO<sub>2</sub> Activated Biochar from Solid Wastes of a Beer Industry and Its Application for Methylene Blue Adsorption. *Waste Manag.* **2018**, *78*, 630–638. [[CrossRef](#)]
101. Rijo, B.; Paula, A.; Dias, S.; Ramos, M.; Ameixa, M. Valorization of Forest Waste Biomass by Catalyzed Pyrolysis. *Energy* **2022**, *243*, 122766. [[CrossRef](#)]
102. Mishra, R.K.; Lu, Q.; Mohanty, K. Thermal Behaviour, Kinetics and Fast Pyrolysis of Cynodon Dactylon Grass Using Py-GC/MS and Py-FTIR Analyser. *J. Anal. Appl. Pyrolysis* **2020**, *150*, 104887. [[CrossRef](#)]
103. Shi, J.; Xing, D.; Li, J. FTIR Studies of the Changes in Wood Chemistry from Wood Forming Tissue under Inclined Treatment. *Energy Procedia* **2012**, *16*, 758–762. [[CrossRef](#)]
104. Bentes, V.L.I.; Nobre, F.X.; Barros, I.C.L.; Couceiro, P.R.C. Composite of Iron Phosphate-Supported Carbon from the Açai (Euterpe Oleracea) as a Solid Catalyst for Photo-Fenton Reactions. *Environ. Nanotechnol. Monit. Manag.* **2021**, *16*, 100520. [[CrossRef](#)]
105. Li, C.; Sun, Y.; Yi, Z.; Zhang, L.; Zhang, S.; Hu, X. Co-Pyrolysis of Coke Bottle Wastes with Cellulose, Lignin and Sawdust: Impacts of the Mixed Feedstock on Char Properties. *Renew. Energy* **2022**, *181*, 1126–1139. [[CrossRef](#)]
106. Faria, J.P.; Arellano, D.B.; Grimaldi, R.; Silva, L.D.C.R.; Vieira, R.F.; Silva, D.D.B.; Agostini-costa, T.D.S. Chemical Characterization of Nut of Butia Capitata Var Capitata. *Rev. Bras. Frutic.* **2008**, *30*, 549–552. [[CrossRef](#)]
107. Kobelnik, M.; Fontanari, G.G.; Marques, M.R.; Ribeiro, C.A.; Crespi, M.S. Thermal Behavior and Chromatographic Characterization of Oil Extracted from the Nut of the Butia (Butia Capitata). *J. Therm. Anal. Calorim.* **2016**, *123*, 2517–2522. [[CrossRef](#)]
108. Peralta, S.L.; Carvalho, P.H.A.; van de Sande, F.H.; Pereira, C.M.P.; Piva, E.; Lund, R.G. Self-Etching Dental Adhesive Containing a Natural Essential Oil: Anti-Biofouling Performance and Mechanical Properties. *Biofouling* **2013**, *29*, 345–355. [[CrossRef](#)]
109. De Conto, D.; Silvestre, W.P.; Baldasso, C.; Godinho, M. Performance of Rotary Kiln Reactor for the Elephant Grass Pyrolysis. *Bioresour. Technol.* **2016**, *218*, 153–160. [[CrossRef](#)]
110. Chang, G.; Huang, Y.; Xie, J.; Yang, H.; Liu, H.; Yin, X.; Wu, C. The Lignin Pyrolysis Composition and Pyrolysis Products of Palm Kernel Shell, Wheat Straw, and Pine Sawdust. *Energy Convers. Manag.* **2016**, *124*, 587–597. [[CrossRef](#)]
111. Soltani, N.; Bahrami, A.; González, L.A. Review on the Physicochemical Treatments of Rice Husk for Production of Advanced Materials. *Chem. Eng. J.* **2015**, *264*, 899–935. [[CrossRef](#)]
112. Teixeira, V.G.; Coutinho, F.M.B.; Gomes, A.S. Principais Métodos de Caracterização Da Porosidade de Resinas à Base de Divinilbenzeno. *Quím. Nova* **2001**, *24*, 808–818. [[CrossRef](#)]
113. IUPAC. Manual of Symbols and Terminology for Physicochemical Quantities and Units, Appendix II: Definitions, Terminology and Symbols in Colloid and Surface Chemistry. *Pure Appl. Chem.* **1972**, *31*, 577–638. [[CrossRef](#)]
114. Ambroz, F.; Macdonald, T.J.; Martis, V.; Parkin, I.P. Evaluation of the BET Theory for the Characterization of Meso and Microporous MOFs. *Small Methods* **2018**, *2*, 1800173. [[CrossRef](#)]
115. Darmawan, S.; Wistara, N.J.; Pari, G.; Maddu, A.; Syafii, W. Characterization of Lignocellulosic Biomass as Raw Material for the Production of Porous Carbon-Based Materials. *BioResources* **2016**, *11*, 3561–3574. [[CrossRef](#)]
116. Cagnon, B.; Py, X.; Guillot, A.; Stoeckli, F.; Chambat, G. Contributions of Hemicellulose, Cellulose and Lignin to the Mass and the Porous Properties of Chars and Steam Activated Carbons from Various Lignocellulosic Precursors. *Bioresour. Technol.* **2009**, *100*, 292–298. [[CrossRef](#)]
117. Daud, W.M.A.W.; Ali, W.S.W. Comparison on Pore Development of Activated Carbon Produced from Palm Shell and Coconut Shell. *Bioresour. Technol.* **2004**, *93*, 63–69. [[CrossRef](#)]
118. Danish, M.; Hashim, R.; Ibrahim, M.N.M. Optimized Preparation for Large Surface Area Activated Carbon from Date (*Phoenix dactylifera* L.) Stone Biomass. *Biomass Bioenergy* **2014**, *61*, 167–178. [[CrossRef](#)]
119. Peterson, S.C.; Jackson, M.A.; Kim, S.; Palmquist, D.E. Increasing Biochar Surface Area: Optimization of Ball Milling Parameters. *Powder Technol.* **2012**, *228*, 115–120. [[CrossRef](#)]
120. Zhang, Y.; Qin, J.; Yi, Y. Biochar and Hydrochar Derived from Freshwater Sludge: Characterization and Possible Applications. *Sci. Total Environ.* **2021**, *763*, 144550. [[CrossRef](#)]
121. Manera, C.; Perondi, D.; Godinho, M. Production of Micro-Mesoporous Activated Carbons from Various Citrus Waste. In Proceedings of the IV Congresso Internacional de Biomassa, Curitiba, Brazil, 25–27 June 2019.
122. Mohan, D.; Rajput, S.; Singh, V.K.; Steele, P.H.; Pittman, C.U. Modeling and Evaluation of Chromium Remediation from Water Using Low Cost Bio-Char, a Green Adsorbent. *J. Hazard. Mater.* **2011**, *188*, 319–333. [[CrossRef](#)] [[PubMed](#)]
123. Li, S.-Q.; Yao, Q.; Wen, S.-E.; Chi, Y.; Yan, J.-H. Properties of Pyrolytic Chars and Activated Carbons Derived from Pilot-Scale Pyrolysis of Used Tires. *J. Air Waste Manag. Assoc.* **2005**, *55*, 1315–1326. [[CrossRef](#)] [[PubMed](#)]
124. Botomé, M.L.; Poletto, P.; Junges, J.; Perondi, D.; Dettmer, A.; Godinho, M. Preparation and Characterization of a Metal-Rich Activated Carbon from CCA-Treated Wood for CO<sub>2</sub> Capture. *Chem. Eng. J.* **2017**, *321*, 614–621. [[CrossRef](#)]
125. Sabri, M.A.; Al Jitan, S.; Bahamon, D.; Vega, L.F.; Palmisano, G. Current and Future Perspectives on Catalytic-Based Integrated Carbon Capture and Utilization. *Sci. Total Environ.* **2021**, *790*, 148081. [[CrossRef](#)]
126. Zhang, X.; Cao, L.; Xiang, W.; Xu, Y.; Gao, B. Preparation and Evaluation of Fine-Tuned Micropore Biochar by Lignin Impregnation for CO<sub>2</sub> and VOCs Adsorption. *Sep. Purif. Technol.* **2022**, *295*, 121295. [[CrossRef](#)]
127. Wjihi, S.; Aouaini, F.; Erto, A.; Balsamo, M.; Lamine, A. Ben Advanced Interpretation of CO<sub>2</sub> Adsorption Thermodynamics onto Porous Solids by Statistical Physics Formalism. *Chem. Eng. J.* **2021**, *406*, 126669. [[CrossRef](#)]

128. Heidari, A.; Younesi, H.; Rashidi, A.; Ghoreyshi, A.A. Adsorptive Removal of CO<sub>2</sub> on Highly Microporous Activated Carbons Prepared from Eucalyptus Camaldulensis Wood: Effect of Chemical Activation. *J. Taiwan Inst. Chem. Eng.* **2014**, *45*, 579–588. [[CrossRef](#)]
129. Du, X.; Cheng, Y.; Liu, Z.; Hou, Z.; Wu, T.; Lei, R.; Shu, C. Study on the Adsorption of CH<sub>4</sub>, CO<sub>2</sub> and Various CH<sub>4</sub>/CO<sub>2</sub> Mixture Gases on Shale. *Alex. Eng. J.* **2020**, *59*, 5165–5178. [[CrossRef](#)]
130. Singh, J.; Basu, S.; Bhunia, H. CO<sub>2</sub> Capture by Modified Porous Carbon Adsorbents: Effect of Various Activating Agents. *J. Taiwan Inst. Chem. Eng.* **2019**, *102*, 438–447. [[CrossRef](#)]
131. Li, M.; Xiao, R. Preparation of a Dual Pore Structure Activated Carbon from Rice Husk Char as an Adsorbent for CO<sub>2</sub> Capture. *Fuel Process. Technol.* **2019**, *186*, 35–39. [[CrossRef](#)]
132. TAPPI T 204 Cm-97; Solvent Extractives of Wood and Pulp. Tappi Press: Atlanta, GA, USA, 1997.
133. ASTM. Standard Practice for Proximate Analysis of Coal and Coke. In *Annual Book of ASTM Standards*; ASTM International: West Conshohoken, PA, USA, 1993; pp. D3172–D3189.
134. Van Soest, P.J.; Wine, R.H. Determination of Lignin and Cellulose in Acid-Detergent Fiber with Permanganate. *J. AOAC Int.* **1968**, *51*, 780–785. [[CrossRef](#)]
135. Singh, G.; Kim, I.Y.; Lakhi, K.S.; Srivastava, P.; Naidu, R.; Vinu, A. Single Step Synthesis of Activated Bio-Carbons with a High Surface Area and Their Excellent CO<sub>2</sub> Adsorption Capacity. *Carbon N. Y.* **2017**, *116*, 448–455. [[CrossRef](#)]
136. Nasri, N.S.; Hamza, U.D.; Ismail, S.N.; Ahmed, M.M.; Mohsin, R. Assessment of Porous Carbons Derived from Sustainable Palm Solid Waste for Carbon Dioxide Capture. *J. Clean. Prod.* **2014**, *71*, 148–157. [[CrossRef](#)]
137. Wedler, C.; Span, R. A Pore-Structure Dependent Kinetic Adsorption Model for Consideration in Char Conversion—Adsorption Kinetics of CO<sub>2</sub> on Biomass Chars. *Chem. Eng. Sci.* **2021**, *231*, 116281. [[CrossRef](#)]
138. Ello, A.S.; De Souza, L.K.C.; Trokourey, A.; Jaroniec, M. Coconut Shell-Based Microporous Carbons for CO<sub>2</sub> Capture. *Microporous Mesoporous Mater.* **2013**, *180*, 280–283. [[CrossRef](#)]
139. Conte, G.; Stelitano, S.; Policicchio, A.; Minuto, F.D.; Lazzaroli, V.; Galiano, F.; Agostino, R.G. Assessment of Activated Carbon Fibers from Commercial Kevlar<sup>®</sup> as Nanostructured Material for Gas Storage: Effect of Activation Procedure and Adsorption of CO<sub>2</sub> and CH<sub>4</sub>. *J. Anal. Appl. Pyrolysis* **2020**, *152*, 104974. [[CrossRef](#)]
140. Singh, G.; Kim, I.Y.; Lakhi, K.S.; Joseph, S.; Srivastava, P.; Naidu, R.; Vinu, A. Heteroatom Functionalized Activated Porous Biocarbons and Their Excellent Performance for CO<sub>2</sub> Capture at High Pressure. *J. Mater. Chem. A* **2017**, *5*, 21196–21204. [[CrossRef](#)]
141. Choi, S.W.; Tang, J.; Pol, V.G.; Lee, K.B. Pollen-Derived Porous Carbon by KOH Activation: Effect of Physicochemical Structure on CO<sub>2</sub> Adsorption. *J. CO<sub>2</sub> Util.* **2019**, *29*, 146–155. [[CrossRef](#)]
142. Serafin, J.; Narkiewicz, U.; Morawski, A.W.; Wróbel, R.J.; Michalkiewicz, B. Highly Microporous Activated Carbons from Biomass for CO<sub>2</sub> Capture and Effective Micropores at Different Conditions. *J. CO<sub>2</sub> Util.* **2017**, *18*, 73–79. [[CrossRef](#)]
143. Bae, J.S.; Su, S. Macadamia Nut Shell-Derived Carbon Composites for Post Combustion CO<sub>2</sub> Capture. *Int. J. Greenh. Gas Control* **2013**, *19*, 174–182. [[CrossRef](#)]
144. Zhu, X.L.; Wang, P.Y.; Peng, C.; Yang, J.; Yan, X. Bin Activated Carbon Produced from Paulownia Sawdust for High-Performance CO<sub>2</sub> Sorbents. *Chin. Chem. Lett.* **2014**, *25*, 929–932. [[CrossRef](#)]
145. Labus, K.; Gryglewicz, S.; Machnikowski, J. Granular KOH-Activated Carbons from Coal-Based Cokes and Their CO<sub>2</sub> Adsorption Capacity. *Fuel* **2014**, *118*, 9–15. [[CrossRef](#)]
146. Quan, C.; Wang, H.; Jia, X.; Gao, N. Effect of Carbonization Temperature on CO<sub>2</sub> Adsorption Behavior of Activated Coal Char. *J. Energy Inst.* **2021**, *97*, 92–99. [[CrossRef](#)]
147. Ello, A.S.; De Souza, L.K.C.; Trokourey, A.; Jaroniec, M. Development of Microporous Carbons for CO<sub>2</sub> Capture by KOH Activation of African Palm Shells. *J. CO<sub>2</sub> Util.* **2013**, *2*, 35–38. [[CrossRef](#)]
148. Cong, H.; Zhang, M.; Chen, Y.; Chen, K.; Hao, Y.; Zhao, Y.; Feng, L. Highly Selective CO<sub>2</sub> Capture by Nitrogen Enriched Porous Carbons. *Carbon N. Y.* **2015**, *92*, 297–304. [[CrossRef](#)]
149. Hao, W.; Björkman, E.; Lilliestråle, M.; Hedin, N. Activated Carbons Prepared from Hydrothermally Carbonized Waste Biomass Used as Adsorbents for CO<sub>2</sub>. *Appl. Energy* **2013**, *112*, 526–532. [[CrossRef](#)]
150. Pramanik, P.; Patel, H.; Charola, S.; Neogi, S.; Maiti, S. High Surface Area Porous Carbon from Cotton Stalk Agro-Residue for CO<sub>2</sub> adsorption and Study of Techno-Economic Viability of Commercial Production. *J. CO<sub>2</sub> Util.* **2021**, *45*, 101450. [[CrossRef](#)]
151. Parshetti, G.K.; Chowdhury, S.; Balasubramanian, R. Biomass Derived Low-Cost Microporous Adsorbents for Efficient CO<sub>2</sub> Capture. *Fuel* **2015**, *148*, 246–254. [[CrossRef](#)]
152. Song, J.; Shen, W.; Wang, J.; Fan, W. Superior Carbon-Based CO<sub>2</sub> Adsorbents Prepared from Poplar Anthers. *Carbon N. Y.* **2014**, *69*, 255–263. [[CrossRef](#)]